University of South-Eastern Norway
Faculty of Technology, Natural Sciences and Maritime Sciences
–

Master's Thesis

Study programme: Master of Science in Micro and Nano Systems Technology

Spring 2023

Omar Saif

Process development for Roll-to-Roll Carbon Nano Tube (CNT) Growth

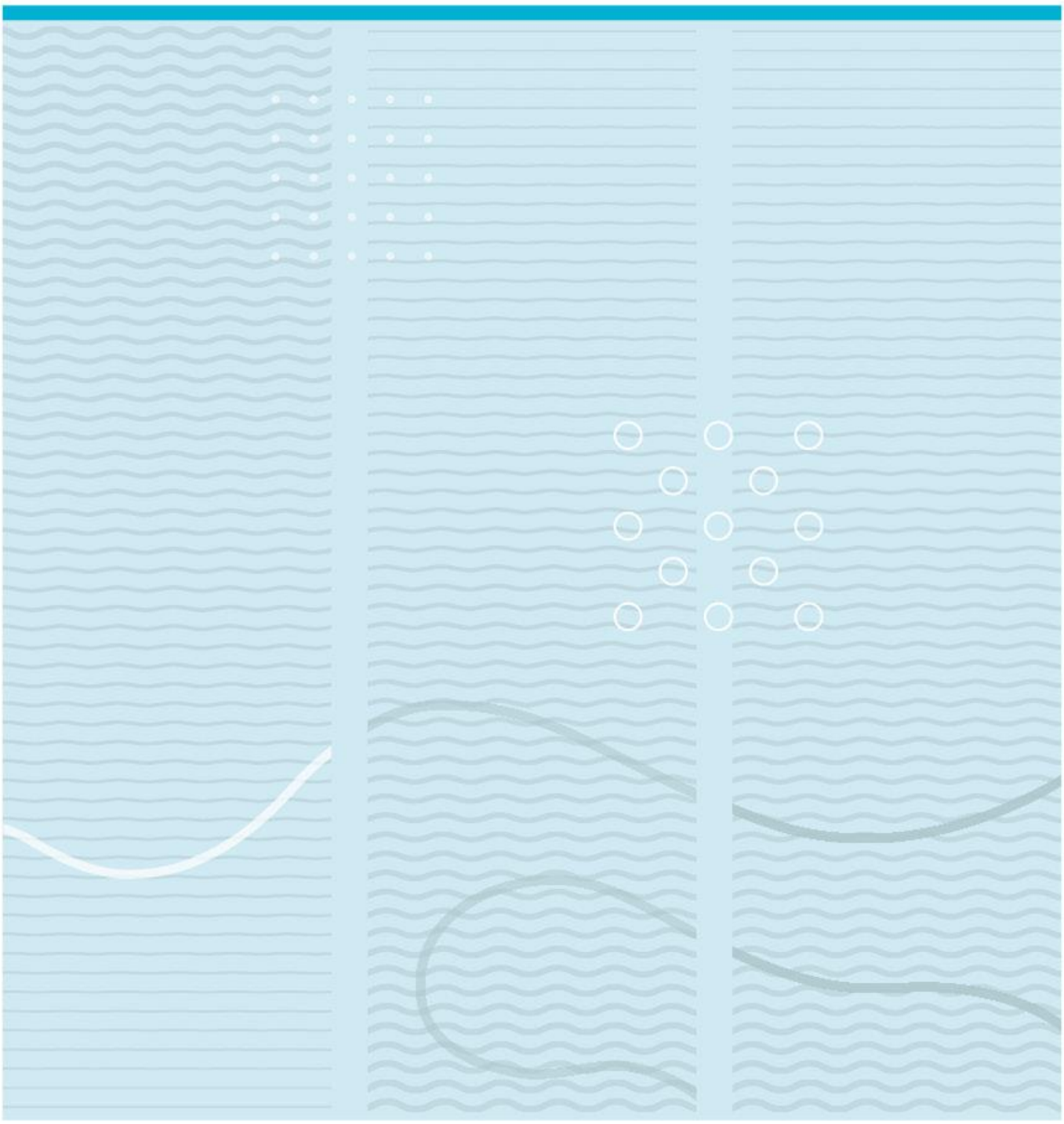

University of South-Eastern Norway
Faculty of Technology, Natural Sciences and Maritime Sciences
Department of Microsystems.
Raveien 215
NO-3184 Borre, Norway

http://www.usn.no

Abstract

This study presents the process development for the synthesis of dense multiwalled carbon nanotube (CNT)- based high energy density electrodes for supercapacitors at pilot scale using an industrial roll-to-roll chemical vapour deposition facility. Pre-etched aluminium foil was used as substrate, where the catalyst nanoparticles of nickel were deposited through sputtering and $NiSO_4$ solution coating methods. The morphology and distribution of Ni nanoparticles and the growth mechanism of carbon nanotubes were studied thoroughly. Atmospheric pressure chemical vapour deposition (AP-CVD) was performed at 580 oC with synthesis time varying from 15 minutes to 180 minutes. This study majorly focused on the study of pilot production facility as it is not only more than 100 times larger in volume than the lab scale CVD reactor, but also possesses several additional challenges that makes it complicated to replicate the synthesis process from lab scale to industrial scale. Hence a systematic investigation of optimal gas ratios, flowrates, concentration, oxide reduction for solution coated samples, heating rate of the sample and segregation of gases was necessary due to the high sensitivity of the CNT growth mechanism to different conditions. Under optimal gas concentration and synthesis time it was possible to achieve high energy dense CNT electrodes with a record-high gravimetric capacitance of 78 F/g and areal capacitance of 1253 mF/cm², whereas the best/state-of-the-art industrial values are 60 F/g and 700 mF/cm², respectively, using activated carbon (AC) based electrodes.

Abbreviation

Symbol	Description
CVD	Chemical vapor deposition
APCVD	Atmospheric pressure Chemical vapour deposition
PVD	Physical vapor deposition
Al	Aluminium
Si	Silicon
Ni	Nickel
Fe	Iron
Co	Cobalt
CNT	Carbon nanotube
iCL-CNT	Interconnected cross-linked carbon nanotube
AC	Activated carbon
EDLC	Electric double layer capacitance
C_2H_2	Acetylene
H_2	Hydrogen
Ar	Argon
SEM	Scanning electron microscopy
FESEM	Field emission scanning electron microscopy
EDS/EDX	Energy Dispersive X-ray Spectroscopy
FTIR	Fourier-transform infrared spectroscopy

Contents

Foreword

This thesis upholds the pinnacle of my Joint International Master in Smart Systems Integrated Solutions (SSIs) at the University of South-Eastern Norway (USN) along with the support of Aalto University (Finland) and Budapest University of Technology and Economics (Hungary) as program universities. The completion of the thesis would not have been possible without the immense support and guidance from my supervisor, Dr. Xuyuan Chen, and co-supervisor, Dr. Raghunandan Ummethala.

Moreover, I would like to offer my gratitude towards the Lab Engineers and Researchers at USN who helped and trained me effectively to carry out my research work successfully.

This thesis was conducted along with the collaboration of nanoCaps AS which provided me the industrial setup and profound knowledge regarding Supercapacitor industry.

I would also like to mention and appreciate all my instructors from all three Universities for guiding me and sharing their knowledge during my diversified course curriculum.

<Vestfold, Norway/03/07/2023>
<Omar Saif>

1 Introduction

1.1 Scope of the Thesis, Motivation and Challenges

Due to rising worldwide energy consumption and the need for renewable energy integration, the need for efficient and sustainable energy storage systems has risen tremendously in recent years. Energy storage is critical for overcoming the intermittent nature of renewable energy sources and providing backup power during high demand periods. Due to their high-power density, fast charging/discharging capability, extended cycle life, and environmental friendliness, supercapacitors have emerged as a promising alternative among various energy storage technologies.

Supercapacitors, also known as ultracapacitors or electrochemical capacitors, are energy storage devices that lie between standard capacitors and batteries. In contrast to batteries, which store energy chemically, supercapacitors store energy electrostatically, allowing for quick energy storage and release. This distinguishing feature makes them appropriate for high-power-delivery applications such as electric vehicles, renewable energy systems, portable devices, and grid stabilization.

The focus of this study is on developing high-performance electrodes for Electric Double-Layer Capacitor (EDLC). EDLC electrodes are widely recognized for their ability to rapidly store and distribute energy, making them excellent candidates for applications needing high power densities. Unlike batteries, which store energy through chemical reactions, EDLCs store energy by ion adsorption at the electrode-electrolyte interface. This charge storage mechanism, known as the electric double layer, enables rapid ion diffusion and efficient energy storage. As a result of its high specific surface area and superior electrical conductivity, activated carbon is often utilized as the electrode material in EDLCs.

The most significant component of a supercapacitor is the electrode material, which stores energy by ion adsorption at the electrode-electrolyte interface. Carbon nanotubes (CNTs) have lately gained popularity as electrode materials for supercapacitors. AC electrodes are frequently utilized and have an areal capacitance of about 700 mF/cm2. The motivation of this study was to outperform AC electrodes in terms of areal capacitance and energy density in order to match with the revised energy and power requirements of modern times. It has been shown recently that CNT electrodes can attain higher areal capacitance by increasing the carpet height and surface area of the

electrode. The current investigation primarily addresses the synthesis and application of such electrodes on a pilot/industrial level in order to prove their outstanding performance, combined with the proof of commercial viability. It will be demonstrated in this thesis that it is possible to achieve almost double the areal capacitance compared to the state-of-the-art AC electrodes by optimal growth conditions and utilization of the pilot production facility. This significant increase in areal capacitance emphasizes the outstanding characteristics of CNTs, such as their high conductivity and large surface area which was also the core motivation for this study.

High-quality CNT growth is critical for achieving good supercapacitor performance. Several approaches for CNT synthesis have been established, with chemical vapor deposition (CVD) being one of the most extensively employed. CVD allows for precise control over the growth process, including the selection of catalyst, growth temperature, and gas composition, allowing for the creation of CNTs with customized properties.

The fundamental approach of this thesis is to develop synthesis process and explore the effect of various growth parameters on the growth of CNTs and their subsequent performance in a supercapacitor through a pilot production or industrial scale facility. Compared to a typical lab scale reactor, the volume of the pilot-scale reactor is more than 100 times. Moreover, several variables were present related to this facility which contributed to additional challenges in developing the optimum synthesis parameters. Firstly, the lab-scale reactors usually have a negligible volume of cold zones that hardly affect the gas distribution in the hot zone. In contrast to this, the specialized design of the large-scale reactor gives rise to different zones ranging from large ‘hot zones’ (580°C) to equally large ‘cold zones’ (room temperature). There is a possibility of segregation of gases as a result of this diverse distribution of temperature where the precursors are released in the cold zones. Moreover, the density of the gases varied hugely in the large scale reactor along the length of facility because of the temperature difference. In addition to this discrepancy, although it was possible to maintain the same proportion of gases used in the lab reactor, it was not possible to match the same flowrate per area as it is for the lab scale machine. In order to overcome these challenges, several approaches were tried, which includes readjusting the gas ratios, increasing the flowrate per area, volume modification of the active zone, inclusion of water vapor, increasing the

turbulence of gases inside the reactor and releasing the gas mixture directly into the hot zone to ensure better mixing.

1.2 Research Approach

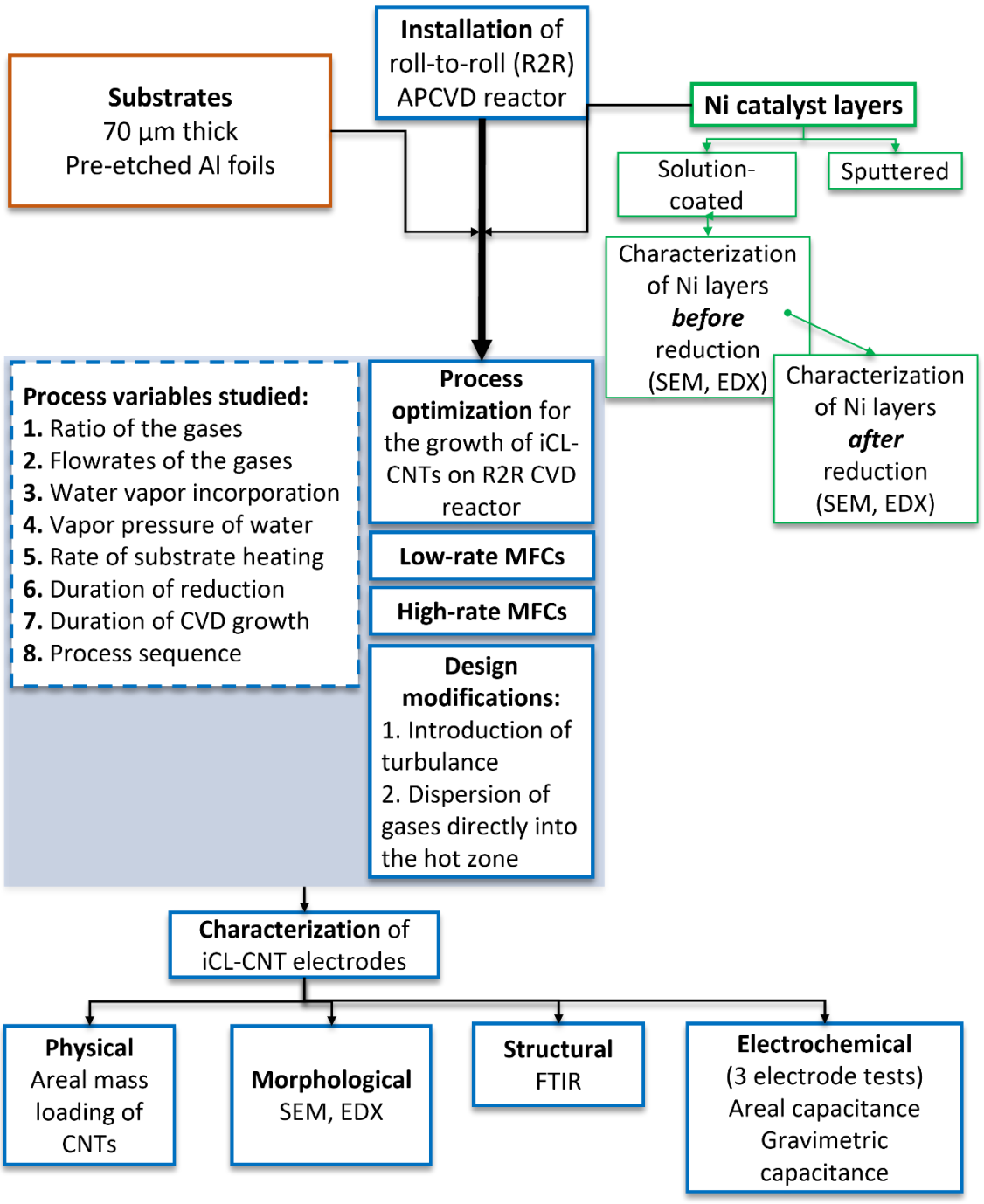

Figure 1-1The research approach and overall workflow of the thesis

The process development for large-scale production of iCL-CNT (Interconnected Cross-linked) electrodes began with the right way of installation of the reactor with regards to the effective transport of gases, ports for cooling water circulation, ventilation of the room and designing safe operation protocols (reduction of risks, minimizing contamination of the floor with carbon nanotubes). The overall workflow of this thesis is clearly elucidated in Figure 1-1.

This research seeks to contribute to the development of optimum growth methods for high-performance supercapacitor electrodes by thoroughly examining the growth conditions and characterizing the as-grown CNTs. The outcomes of this work will help to better understand the relationship between CNT growth parameters and supercapacitor performance, allowing to (a) design large volume production facilities for iCL-CNT electrodes and (2) manufacture more efficient and sustainable energy storage devices.

1.3 Structure of the thesis

The thesis uses a systematic method to investigate and comprehend the growth parameters and properties of the iCL-CNTs for supercapacitor applications. Chapter 2 presents a literature review on CNTs, Chemical Vapor Deposition (CVD), the common substrate material, catalysts, CNT growth methods, supercapacitor electrodes, and CNT characterization. Chapter 3 covers the sample preparation methods, Atmospheric pressure chemical vapor deposition (APCVD) process parameters, characterization techniques, and electrochemical analysis methods. In Chapter 4, the main findings are discussed, which broadly encompass temperature profiling and gas density distribution in the production facility, modifications in catalyst deposition methods, CVD gas ratios, growth duration, and optimal growth conditions. Finally, the conclusions highlight the most important findings and thus the impact of this study on the technical and commercial frontiers of today's supercapacitors.

2 Literature Review

2.1 Electrodes for Supercapacitors

Supercapacitors, also known as ultracapacitors, offer significant advantages over conventional batteries as electrical energy storage devices. They excel in providing high current and specific power for short durations, even as brief as less than a minute. Some of the key advantages of supercapacitors over conventional lithium-ion batteries include fast charging capability, high power density, longer cycle life due to the absence of reversible chemical reactions, and a wider operating temperature range.

The primary storage mechanisms in supercapacitors are the electric double layer capacitor (EDLC) and the pseudo capacitor, which differentiate them from conventional batteries. The EDLC configuration consists of two electrodes, a separator, and an electrolyte. Activated carbon-based electrodes are commonly used in EDLCs, with metallic collector foils establishing electrical connections between the electrodes and the terminals. A permeable separator membrane is positioned between the electrodes to prevent short circuits. The cell is then infused with an electrolyte, which can be either organic or aqueous, depending on the desired power, voltage, and temperature requirements. Proper sealing of the cell is crucial to maintain its integrity. When a voltage is applied, the ions present in the electrolyte migrate through the electrolyte and accumulate on the surface of the electrodes. This accumulation and separation of ions create a double layer capacitance, which contributes to the storage of electrical charge. In the case of pseudo capacitors, the charge accumulation process involves surface faradic electron charge transfer reactions. During long-term use, reversible reduction and oxidation reactions take place on the electrodes, which may lead to structural changes in the electrodes.

Indeed, the performance of supercapacitors is greatly influenced by the choice of electrode material and electrolyte. While AC) based electrodes are commonly used in supercapacitors, they do have limitations. AC electrodes often exhibit low mesoporosity, which restricts the accessibility of the electrolyte and limits the energy density of the device. This, in turn, leads to poor electrical conductivity, high internal resistance, and low power density. CNTs present a promising alternative to address these challenges. CNT-based electrodes offer several advantages over AC electrodes. One key advantage is

their high mesoporosity, which allows for greater accessibility of the electrolyte. This improved electrolyte accessibility enhances the charge storage capacity and enables higher energy density in supercapacitors. Furthermore, CNTs possess a large surface area, which provides ample space for charge accumulation. This results in higher capacitance and improved energy storage capabilities. Additionally, CNTs exhibit superior electrical properties, such as high electrical conductivity, which facilitates efficient charge transfer and lowers the internal resistance of the supercapacitor. The reduced internal resistance enables faster charge-discharge rates and higher power density, making CNT-based supercapacitors suitable for applications requiring rapid energy delivery [1]-[4].

2.2 Carbon nanotube (CNT)

Prior to 1980, the most well-known carbon forms were diamond, graphite, and amorphous carbon. However, our understanding of carbon has grown to include all its forms. Kroto et al. found a new kind of fullerene in 1985 [5], while Iijima and his research group discovered carbon nanotubes (CNTs) in 1991 [6]. CNTs have gotten a lot of attention in research and applications because of their remarkable properties, such as their length, which can approach microns, and their nano-meter scale diameter, which results in a high aspect ratio. CNTs have a cylindrical shape with sp2-hybridized carbon atoms arranged hexagonally [7]. Until 1993 it was believed that CNTs have a hollow interior structure made up of one or more layers of graphene sheets. However, in 1993 it was being discovered that CNTs are made of single layer of graphene [8]-[9].

In general, CNTs are divided into three types based on their inner walls (Figure 2-1). The earliest type of carbon nanotube is single-walled carbon nanotubes (SWNTs), which are made up of a single graphene layer with a diameter of 1-2 nm [8]. Catalysts are frequently employed in the creation of nanotubes to control the length and purity of the nanotubes.

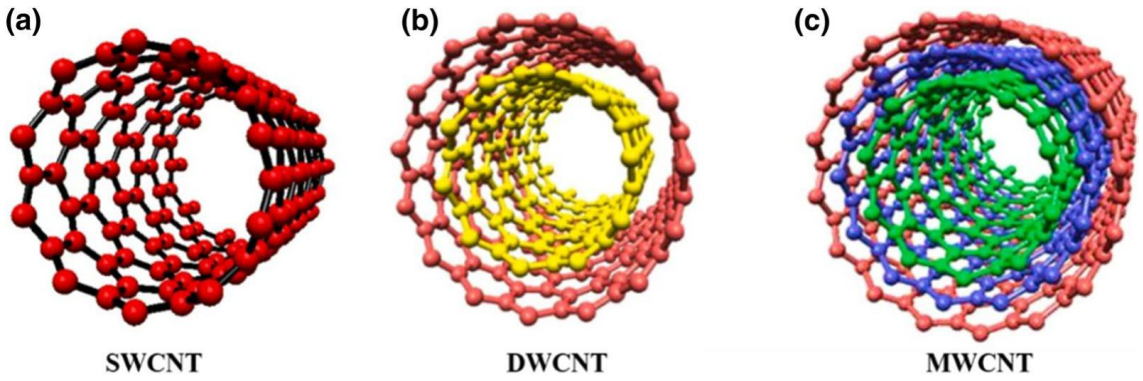

Figure 2-1 Structure of (a) single-walled carbon nanotubes, (b) double-walled carbon nanotubes, and (c) multi-walled carbon nanotubes [10]

The second type of carbon nanotube is double-walled carbon nanotubes (DWNTs), which are made up of two carbon nanotubes with the outer tube surrounding the inner tube. The outer diameter of DWNTs is 2-4 nm and the inner diameter is 1-3 nm [7].

The third type of carbon nanotube is multi-walled carbon nanotubes (MWNTs), which are made up of many layers of graphene sheets coiled into tubes. MWNTs have diameters ranging from 2 to 50 nm and are designated and numbered based on the presence of graphene sheets [11].

2.3 Chemical Vapour Deposition (CVD)

Chemical Vapor Deposition (CVD) is a popular process for depositing thin films on heated surfaces by chemical reactions involving gas-phase precursors. Due to the utilization of chemical processes, CVD offers advantages such as tuneable deposition rates and high-quality conformal coatings over physical vapor deposition approaches.

Controlling the structures and properties of the deposited materials is possible with CVD, leading to a variety of advanced systems such as plasma-enhanced CVD [12], metal-organic CVD [13] and many others. CVD may be performed under atmospheric pressure, as opposed to high-vacuum procedures, making it prominent in electronics, optoelectronics, surface modification, and biological applications.

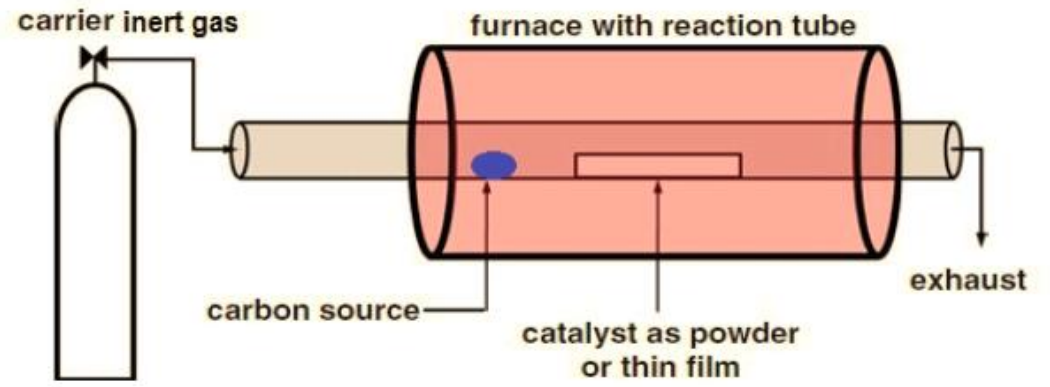

Figure 2-2 General schematic of chemical vapor deposition [16]

The basic process of CVD consists of several steps (Figure 2-2), including vacuuming the chamber and tube, the transport of reactant gases into the reactor, heating, gas-phase reactions, adsorption of gases and intermediates onto the substrate surface, heterogeneous reactions at the gas-solid interface leading to film formation, and by-product desorption and cooling [14], [15].

Moving to the types of different types of CVD processes which are illustrated in Figure 2-3. Here Low-Pressure Chemical Vapor Deposition (LP-CVD), Plasma-Enhanced Chemical Vapor Deposition (PE-CVD), Metal–Organic Chemical Vapor Deposition (MO-CVD) are processes in low pressure only whereas Thermal Atomic Layer Deposition (ALD) and Plasma-Enhanced Atomic Layer Deposition (PE-ALD) can be done in low and atmospheric pressure.

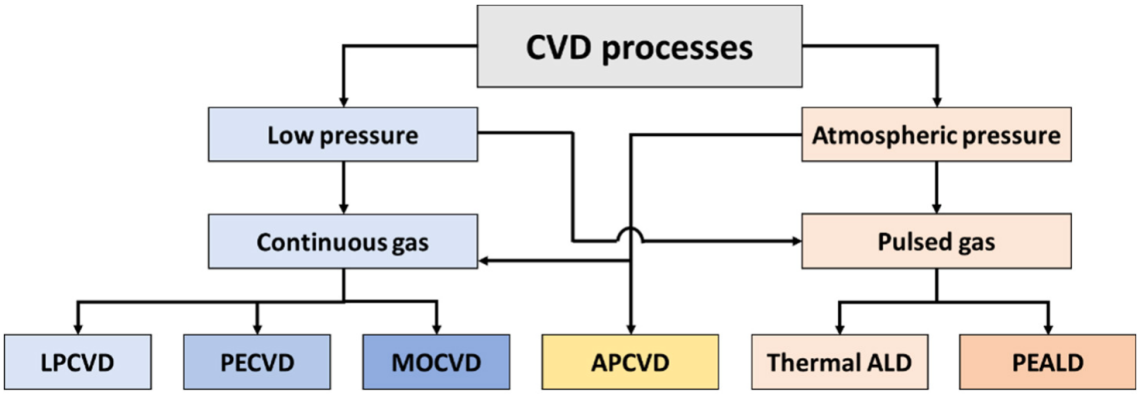

Figure 2-3 Different types of CVD processes [17]

Among these approaches, Atmospheric Pressure Chemical Vapor Deposition (APCVD) was used in this study. APCVD, unlike other CVD technologies, only works at or near

atmospheric pressure. In APCVD, the precursors might be volatile liquids or low-melting solids that are transported to the reaction location by a carrier gas. Within the reaction chamber, two types of reactions occur: homogeneous reactions in the vapor phase and heterogeneous reactions at the vapor-solid boundary. When depositing dense films and coatings, the process parameters are modified to induce heterogeneous reactions. For the creation of porous coatings, a combination of heterogeneous and homogeneous gas phase process is preferred [18].

In the APCVD process for CNT growth, a thin layer of catalyst is deposited on the surface of the substrate. The catalyst-coated substrate is then introduced into the reactor, where it is exposed to a carbon-based gas, such as acetylene or ethylene, which acts as the feedstock for CNT formation. The carbon gas decomposes on the catalyst surface, leading to the emergence of carbon clusters. As carbon atoms continue to be added to these clusters, they expand and eventually adopt a cylindrical shape, resulting in the formation of CNTs. The growth of the nanotubes generally occurs parallel to the axis of the catalyst particle. During the growth process, the catalyst particle gradually becomes covered by carbon compounds, which reduces its activity. To sustain CNT growth, it is crucial to reactivate the catalyst by removing the accumulated carbon compounds from its surface. This is achieved by introducing hydrogen gas into the reactor, which reacts with the carbon molecules and facilitates their removal from the catalyst surface.

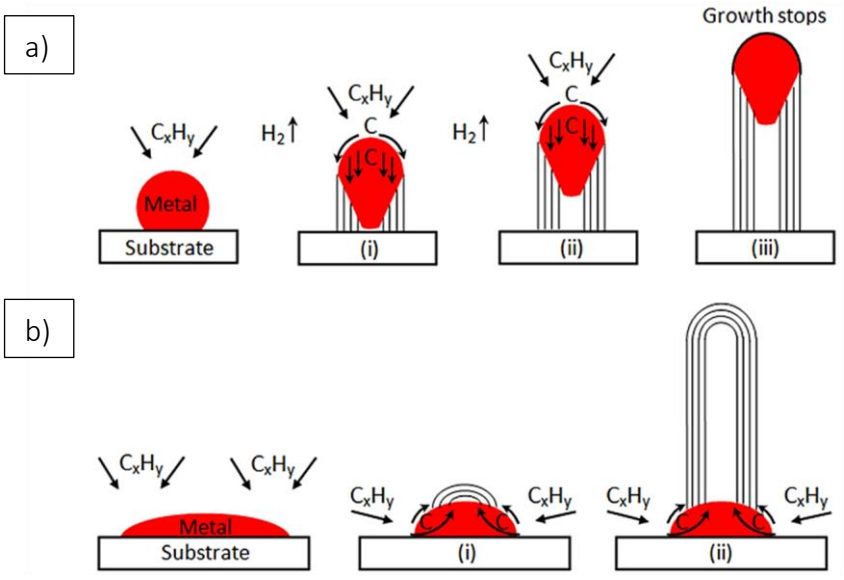

Figure 2-4 CNT growth mechanism a) tip growth and b) root growth [21]

The mechanism of CNT growth involves two distinct processes known as tip growth and root growth (Figure 2-4). Tip growth occurs when the metal catalyst has weak interaction with the substrate. In this mechanism, carbon derived from hydrocarbons decomposes and diffuses from the metal catalyst to its bottom region, where it precipitates between the substrate and the catalyst. This promotes the growth of the entire catalyst nanoparticle, and the process continues until the metal particle becomes entirely covered with an excess of carbon, leading to growth termination, referred to as tip growth. In contrast, root growth occurs when the catalyst and substrate have a strong interaction. In this case, the carbon precipitates from the top of the metal without pushing up the metal particles. This phenomenon is known as root growth. Regardless of the growth model, whether tip growth or root growth, it is important to note that the catalyst particle serves as the starting point for CNT growth, providing the necessary nucleation site and serving as a template for the formation of the nanotube [19]-[21].

2.4 Substrate

The substrate material chosen is critical for the quality and yield of carbon nanotubes (CNTs) during the growing process. The material, surface shape, and textural qualities of the substrate have a major impact on the resultant CNTs as the substrate not only acts as a support but also interacts with the catalyst and the growth environment, the catalyst-substrate interaction is a key issue to address. Physical interactions such as Van der Waals and electrostatic forces can limit catalyst particle movement on the substrate, minimizing metal particle diffusion and stabilizing catalyst particle size distribution during CNT synthesis. Chemical interactions between the catalyst and the surface groups of the substrate can also aid in the maintenance of catalyst particle size distribution during CNT development. Chemical vapor deposition (CVD) has been used to develop CNTs on various substrates such as silicon, quartz, and metal-based substrates such as aluminium. The carbon capacity and growth efficiency are affected by the support material used. The direction and orientation of CNT development are influenced by factors such as grain boundaries and crystalline steps on the substrate surface [22]-[25].

2.5 Catalyst for CNT growth

The catalyst plays a crucial role in the growth of high-quality carbon nanotubes (CNTs) and influences their growth characteristics. Transition metal nanoparticles are commonly used as catalysts in the CVD (chemical vapor deposition) process for synthesizing CNTs. The size of the catalyst particle determines the diameter of the resulting nanotubes, as it serves as the nucleation center for their growth.

Transition metals such as iron (Fe), cobalt (Co), and nickel (Ni) have been found to exhibit excellent catalytic activity for CNT growth. This can be attributed to their high solubility for carbon at elevated temperatures and their ability to facilitate the diffusion of carbon atoms. Among these transition metals, Ni catalysts have been observed to promote the growth of aligned CNTs with the best alignment, as well as a smooth and clean wall surface [26].

Ni catalysts offer several advantages in CNT synthesis, including uniform and stable catalytic activity, as well as efficient carbon segregation across the catalyst's surface. These factors contribute to improved CNT alignment during growth. The use of Ni catalysts can result in the production of CNTs with superior properties, making them an attractive choice for various applications [27].

Therefore, the selection of an appropriate catalyst, such as Ni, is a critical factor in achieving desired CNT growth characteristics, including alignment, surface quality, and overall quality of the synthesized nanotubes.

2.6 Catalyst Deposition Methods

The deposition of catalyst as a thin film can be achieved using various methods, each with its own advantages and disadvantages. Some common deposition techniques include sputtering, electron beam evaporation, solution coating, and electrochemical plating. The choice of deposition method depends on the desired outcome and specific requirements of the application. In this study, sputtering and solution coating is being utilized for catalyst deposition.

Sputtering is a physical vapor deposition (PVD) technique where a target material is bombarded with positively charged ions to eject atoms from its surface. This process involves collisions between the incident particles and surface atoms, resulting in the ejection of target atoms with kinetic energy. Sputtering can significantly affect the film

growth kinetics, particle/cluster size, and microstructure. It is commonly used to produce films and coatings [28].

Solution coating, on the other hand, involves the use of a catalyst solution to coat the substrate surface. This method can be carried out through techniques such as drop coating, dip coating, and spray coating. In solution coating, catalyst compounds are dissolved in a suitable solvent, such as ethanol, to prepare the coating solution. The substrate is then subjected to the solution coating process, and the solvent is evaporated, leaving behind a well-coated surface with the catalyst compounds [29].

Overall, the deposition of catalyst as a thin film is a critical step in CNT synthesis, and the selection of an appropriate deposition method is important to achieve the desired catalyst characteristics and optimize the growth of high-quality CNTs.

3 Experiments and Experimental Set-up

3.1 Catalyst preparation

3.1.1 Sputtered Sample

In this study, nickel sputtered samples were used, which were prepared using a DC magnetron sputtering facility, make: AJA International, model ATC 20x20x30. Pre-etched aluminum foils of 70 µm were used as substrates and pure Ni (99.999%) as target. The depositions were carried out at a power of 300 W and a sample rotation speed of 20 turns/minute to ensure better uniformity. The thickness of Ni (as analyzed from a planar reference crystal) is 300 nm.

3.1.2 Solution Coated Sample

Solution-coated samples were prepared by exposing the pre-etched aluminum foil to a 0.1 M $NiSO_4$ in ethanol solution. Four different methods were carried out in order to facilitate the deposition of nickel nanoparticles, which were drop coating, dip coating (single immersion and 4-time immersion) and spray coating.

In order to prepare the 0.1 M $NiSO_4$ solution, the following calculation was followed –

$$\frac{0.1\frac{mol}{L} \times molar\ mass\ of\ NiSO_4\ \left(154.7\frac{g}{mol}\right) \times Volume\ of\ ethanol\ (ml)}{1000\ ml} \quad (1)$$

This process also includes overnight ultrasonic bath to ensure the proper dilution of the solution.

3.1.2.1 Drop-coat

The initial stage in the drop coating procedure is to prepare the necessary dimensions of Al foil, followed by cleaning it with ethanol and allowing it to air-dry. The previously prepared (fresh) $NiSO_4$ solution, together with a petri dish and a sterile pipette, is then put in an ambient temperature fume hood to begin the drop coating process. For this investigation, approximately 38 µl/cm² $NiSO_4$ is used since this amount theoretically amounts to approximately 250 nm Ni layer. The following calculation was used to determine the above volume of $NiSO_4$:

Volume of Ni on top of the substrate = desired layer thickness x area of the substrate

= 250nm x 1 cm^2

Mass of Ni on the substrate = Density of Ni x Volume of Ni

= 8.9 g/cm^3 x 250nm x 1 cm^2

Required $NiSO_4$ solution = mass of Ni on the sample/amount of Ni in 0.1M $NiSO_4$ in 1 ml solution

= 8.9 g/cm^3 x 250nm x 1 cm^2 / 0.00587 g

= 38 µl/cm^2

3.1.2.2 Dip-coat

To begin the dip coating process, the chosen substrates were immersed in the solution using a petri dish. The immersion operation was performed 1 time or 4 times for 5 minutes each to create a consistent coating on both sides of the substrate. Following each dip-coating, the samples were dried passively via hot-plate to allow the ethanol to evaporate. This intermediate drying step was crucial in settling the coating quickly, promoting even layer distribution over the underlying surface.

3.1.2.3 Spray-coat

Spray-coating was attempted because of its ease of scalability, compared to other techniques. However, this method was performed using a conventional spray bottle, where the main focus was to ensure covering the whole surface of the substrate with necessary dimensions with enough amount of the $NiSO_4$ solution. Following that, the sample was air-dried until ethanol is dried completely, leaving behind a uniform deposition of the Ni salt on the substrate.

3.2 APCVD process parameters - Pitot Production Facility

The pilot facility (nearly 2 tons) for the iCL-CNT production was assembled first and then the gas connections with specific mass flow controllers, vacuum system, electrical connections, and cooling water circulation system were established. The heating elements and the quartz tube were baked at about 800 ^oC before the inception of experiments. The synthesis equipment is specifically designed for roll-to-roll processing, enabling the synthesis of carbon nanotubes (CNTs) on flexible substrates with continuous feeding and winding mechanisms. This configuration ensures efficient and scalable

production. The Al foil roll typically ranges from about 100-130 m in length and 0.25 m in width. The equipment is equipped with a temperature control system that enables precise adjustment of the substrate temperature up to 1200 ^{o}C during the deposition process. Maintaining the correct temperature is crucial for controlling the growth and quality of the CNT layer.

Additionally, the equipment includes a detachable RF (radio frequency) plasma generation accessory to provide additional energy for the decomposition of the hydrocarbon precursor. However, it should be noted that this particular study did not utilize plasma-enhanced chemical vapor deposition (PE-CVD).

Furthermore, the equipment features an automated control system, facilitating easy operation and parameter adjustments. This automation enhances the reproducibility and consistency of the CNT synthesis process. With its roll-to-roll configuration, temperature control, and automation capabilities, this equipment is suitable for industrial-scale CNT synthesis.

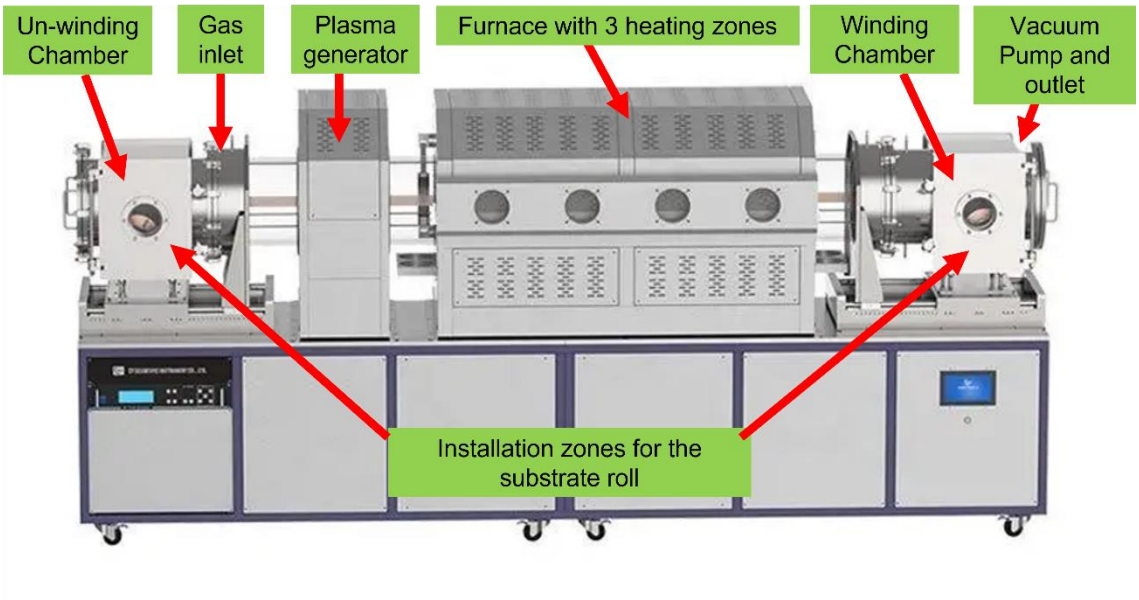

Figure 3-1 Roll-to-Roll pilot Production facility for continuous CNT Synthesis.

As depicted in the Figure 3-1 Roll-to-Roll pilot Production facility for continuous CNT Synthesis.the equipment comprises two chambers, namely the unwinding chamber (left) and the rewinding chamber (right), specifically designed for easy installation of the aluminum foil roll. Both the ends of the quartz tube are mounted with cooling water circulation jackets in order to protect the rubber gaskets that hold the tube firmly in

position and avoid air leakage. The system includes an inlet and outlet dedicated for feedstock gases, with the outlet serving the dual purpose of evacuating the chamber and controlling the pressure, thereby enabling uninterrupted CNT synthesis. To ensure efficient and uniform heating, the furnace is equipped with three separate heating zones, each of which can be independently controlled using the automated control system.

Table 3-1 Parameters utilized regarding APCVD process for CNT synthesis.

Sl	C_2H_2 (SCCM)	H_2 (SCCM)	Ar (SCCM)	Gas Ratio (C_2H_2: H_2 Ar)	Temperature (℃)	Pressure (atm)	CVD duration (min)
1	90	450	180	1:5:2	580	1	180
2	200	1000	400	1:5:2			30-60
3	229	1000	458	1:4.4:2			15-60
4	266	1000	532	1:3.8:2			15-60
5	366	1000	732	1:2.7:2			30-60
6	166	624	332	1:3.8:2			30-60

Table 3-1 presents the process parameters employed in the experiments conducted to investigate the influence of various factors, such as gas ratio, flowrates, and process duration on the yield and quality of the carbon nanotubes (CNT). To ensure the integrity of the substrate, the temperature was precisely set at 580 ^{o}C, considering that the substrate material, namely aluminum, has a low melting point of 660 ^{o}C. By maintaining the temperature within this range, the structural integrity of the thin foil was preserved during the CNT synthesis process.

In the initial phase of the research, the chosen gas ratios were based on adapting the conditions from a lab-scale reactor, which used 20 SCCM C_2H_2, 100 SCCM H_2, and 40 SCCM Ar, to achieve the highest yield of carbon nanotube (CNT) synthesis. These specific values were also selected because they corresponded to the maximum capacity of the available mass flow meters for the precursors.

However, it is important to note that there were significant differences between the lab-scale reactor and the pilot-scale production facility. With the large-scale facility, there

were more variables to consider, making it challenging to replicate the CNT growth conditions precisely. Additionally, the C_2H_2 flowrate per unit area in the lab-scale reactor was 1.37 ml/min/cm² which is 8.5 times larger than the flowrate per unit area in the pilot scale reactor, but the gas ratios were maintained.

Subsequently, when new mass flow meters were installed, the overall flow rate was increased from 0.16 ml/min/cm² to 0.35 ml/min/cm². This adjustment was made while keeping the gas ratios unchanged. To further investigate and observe the effects, the flow rates of C_2H_2 and Ar were increased. However, the proportion of H_2 remained fixed due to the limitations of the mass flowmeter. Eventually, the optimal conditions were determined to be 266 SCCM C_2H_2, 1000 SCCM H_2, and 532 SCCM Ar, with a growth duration of 30 minutes. These optimal conditions were established within the technical constraints posed in the reactor, and also based on achieving the desired CNT growth and supercapacitor performance.

3.3 Tools for Characterization and Analysis

3.3.1 Morphology of CNT and Catalyst Particles

In the morphological study of nickel nanoparticles and synthesized carbon nanotubes (CNTs), both a Hitachi SU 3500 Scanning Electron Microscope (SEM) and a Hitachi SU 8230 Field Emission Scanning Electron Microscope (FESEM) were employed.

The Hitachi SU 3500 SEM was utilized for characterizing the CNTs. This SEM model offers a wide range of magnification options, going up to 300kX. However, for this study, the magnification used ranged from 2kX to 70kX. The accelerating voltage during characterization varied between 5kV and 15 kV. The SEM was operated in the secondary electrons (SE) mode, which provides imaging of the outer shell electrons. This mode was specifically chosen to examine the morphology of the CNTs, including measurements of CNT carpet height, diameter, and distribution characteristics.

On the other hand, the Hitachi SU 8230 FESEM was utilized for characterizing nickel nanoparticles. This FESEM model offers high magnification capabilities, up to 1000kX, resulting in significantly higher resolution images of the sample surface. However, in this study, a highest magnification of 180kX was used. The FESEM was employed to study the

morphology, size, and distribution of the nickel nanoparticles both before and after reduction or heat treatment, as well as before CNT synthesis.

Furthermore, Energy Dispersive X-Ray Spectroscopy (EDX or EDS) was conducted using the FESEM for mapping of the as-deposited substrates, while the same function of the SEM machine was utilized for elemental analysis.

Overall, the combination of the Hitachi SU 3500 SEM and the Hitachi SU 8230 FESEM, along with EDX/EDS analysis, provided comprehensive characterization of both the carbon nanotubes and the nickel nanoparticles in terms of their morphology, size, distribution, and elemental composition.

Furthermore, Fourier-transform infrared spectroscopy (FTIR) was employed to assess the quality of the synthesized carbon nanotubes (CNTs). The FTIR analysis involved the use of a facility equipped with a 1064 nm laser as the excitation source, capable of delivering a maximum power of 0.5 W. By subjecting the synthesized CNTs to FTIR analysis, it becomes possible to gain insights into their structural characteristics such as the carbon-carbon binding states and to assess their overall quality.

3.3.2 Electrochemical Analysis

In the electrochemical analysis of the carbon nanotube (CNT) electrodes, both the 2-electrode method and the 3-electrode method were employed.

For the 2-electrode method, coin cells were prepared using CR2032 cell cases, a stainless-steel spacer (0.5 mm thick) and a stainless steel spring. A pair of Al-CNT electrodes were sandwiched against each other, separated by a glass fiber separator. An organic electrolyte was used as the ionic medium. The coin cell was assembled inside a nitrogen-filled glovebox. The coin cell configuration allows for a simplified setup, where the working electrode and counter electrode are directly connected within the cell (Figure 3-2a).

In contrast, the 3-electrode method was utilized with a more elaborate setup. It involved the use of a 1.0 M Na_2SO_4 aqueous solution as electrolyte, the Al-CNT electrode as the working electrode, standard Ag/AgCl electrode as the reference electrode, and pure graphite as the counter electrode. (Figure 3-2b).

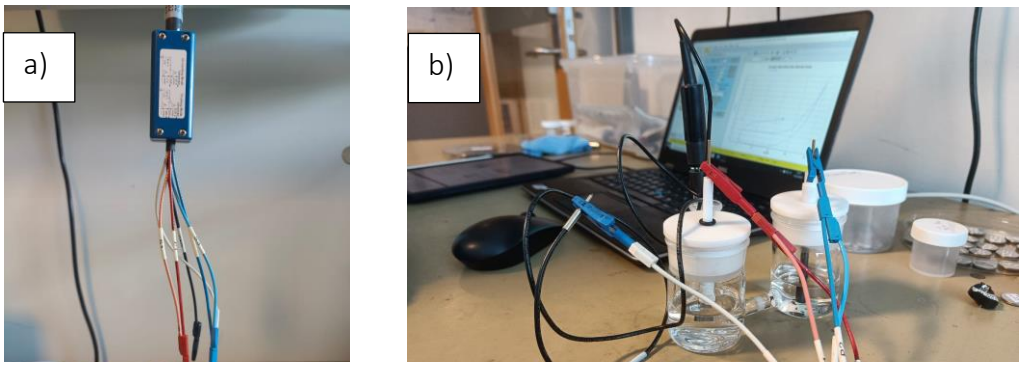

Figure 3-2 Set-up for Electrochemical analysis a) 2-electrode and b) 3-electrode.

The 3-electrode setup was preferred for most of the tests due to its advantages of shorter preparation time and faster measurements. It allowed for efficient screening of electrodes with desirable electrochemical characteristics. Electrodes exhibiting good electrochemical properties, as determined by the 3-electrode method, were selected for further testing and analysis using the 2-electrode setup. The 2-electrode method, involving the coin cells, is considered more reliable for industrial applications. It provides a closer representation of the electrode performance in practical settings.

Overall, the combination of the 3-electrode method for initial screening and the subsequent use of the 2-electrode method with coin cells allowed for a comprehensive assessment of the electrochemical properties of the CNT electrodes, ensuring reliable and practical insights for industrial applications.

4 Results and Discussion

4.1 Temperature Profiling of Pilot Production Facility

High temperature profiling was conducted in the quartz tube before starting the growth optimization experiments to study the actual temperature variation with respect to the temperature displayed on the control panel. For this procedure, standard industrial process was followed where Pico temperature data logger was used with thermocouples. There are three zones for heating which can be controlled independently through the control interface. Tests were done by setting the heating zones at 550 °C to 600 °C and the temperatures at the center (axis) of the quartz tube were measured.

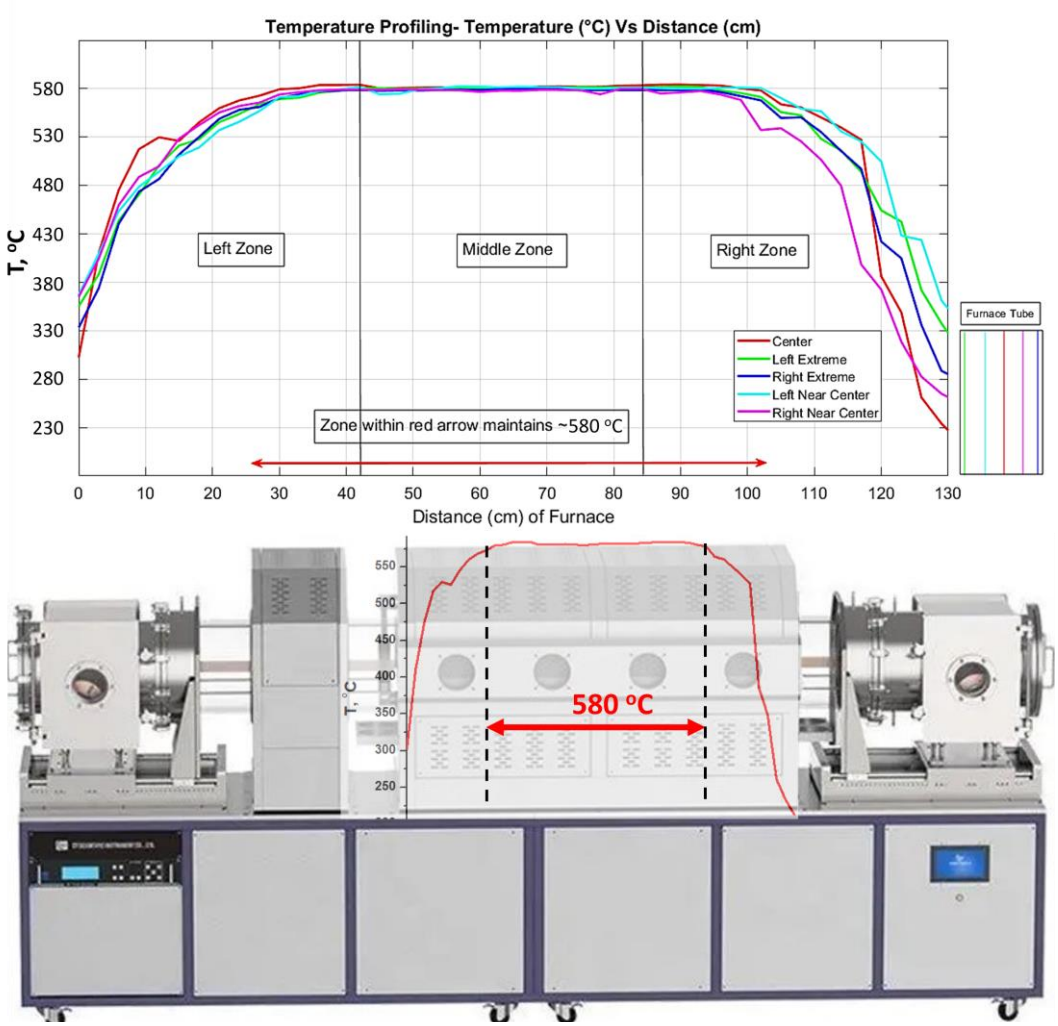

Figure 4-1 Quartz tube temperature profile of pilot production facility

Firstly, it was found that the temperature measured by the thermocouple was 20-22 °C cooler than the temperature displayed on the control panel. The deviation from the set

temperature was observed to be different in different heating zones. So, in order to obtain a homogenous predetermined temperature in the middle of the furnace, each zone was individually calibrated to different set temperatures accounting for the different losses of heat in the corresponding zones. In such way, a recipe was formulated to obtain a maximum uniform temperature zone of about 70 cm in length within a total hot zone of about 120 cm length. The temperature distribution for a measured temperature of 580 °C is shown in Figure 4-1.

4.2 Gas density distribution in Pilot Production Facility

The distance in the quartz tube between the point of release of the gas mixture ($Ar+H_2+C_2H_2$) and the reaction (hot) zone ranges from 40-60 cm in a typical lab-scale CVD reactor of small volume. In this case, this distance is about 140 cm and the expansion volume available for the gas is about 113 times larger than the lab-scale reactor. This results in the existence of huge empty volume in the cold zone of the quartz tube before the gas enters the reaction zone. In addition to this, the feeding chamber on the left side (Figure 3-1) is also a cold zone (maximum temperature of 40^{o}C) with huge volume in comparison to the volume of the reaction zone. Hence, there is a fair chance for the gas mixture to segregate based on their densities and the proportion of gases that enter the hot zone may not match with that of the feedstock. Therefore, the gas distribution methodology was used to determine the nature of distribution of acetylene (C_2H_2) inside the tube when temperature varies.

$$D = PM/RT \quad (2)$$

Here, the modified ideal gas law has been used to determine the density of the gas, where

D= density of the gas

P= pressure, which is 1 atm

M= molar mass of C_2H_2, which is 26.04 g/mol

T= temperature, which is 580°C or 853K

R= ideal gas constant, which is 0.08 L atm / mol K

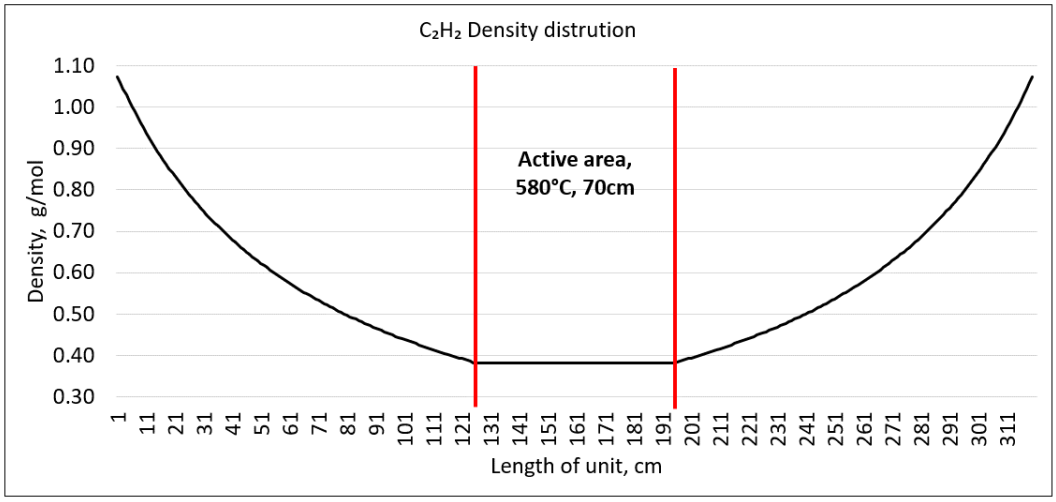

Figure 4-2 Density distribution of C_2H_2 in quartz tube

It has been observed that the density distribution varied significantly in comparison with the lab scale facility where the temperature variation remains between 550°C to 600°C. The same is expected for the rest of the gases in the mixture. As a result, there is a possibility of gas segregation, where it is speculated that the heavier gases such as Ar and C_2H_2 may accumulate more in the cold zones than that enters the hot zone, which will lead to lower deposition rates thereby considerably hindering the CNT growth kinetics and quality.

4.3 Catalyst Deposition Method variation

The mass, morphology, size, spatial distribution, and depth of penetration of the Ni nanoparticles on the Al foil is a critical parameter that influences the growth quality of the carbon nanotubes. Although the morphology of sputtered Ni layers is widely studied, there is no literature addressing the same about Ni reduced from $NiSO_4$ salt solution.

4.3.1 Reduction of Nickel Salt

The growth of CNTs takes place in two stages: (a) reduction of Ni salt into metallic Ni nanoparticles and (b) growth of CNTs from the catalyst nanoparticles. Due to the possible segregation of gases in the pilot production reactor, it needed to be first confirmed that the reduction of nickel salt was carried out properly. Therefore, the as-deposited $NiSO_4$ salt and the salt after reduction treatment (exposure to Ar and H_2 at 580 ^{0}C) were characterized by SEM in both top-view and cross-sectional modes, and by EDS mapping.

From the obtained EDS results (Figure 4-3a), a strong presence of oxygen and sulfur were identified in the nickel salt cluster before the reduction process (denoted by red arrows). As the reduction was performed, nickel salt is expected to decompose in the presence of hydrogen gas and heat, culminating in the creation of NiO (nickel oxide) and following that, the NiO transforms into nickel nanoparticles. The EDX spectrum for the same salt after reduction, shown in (Figure 4-3b) confirms the complete absence of sulfur peak and a significant decline in the oxygen content as well. This suggests that the Ni salt is effectively reduced during the reduction treatment performed before the growth of CNTs. The SEM images in Figure 4-3 further suggests that the reduced Ni crystals show a much smaller size compared to the size of the $NiSO_4$ crystals on the surface of the Al foil.

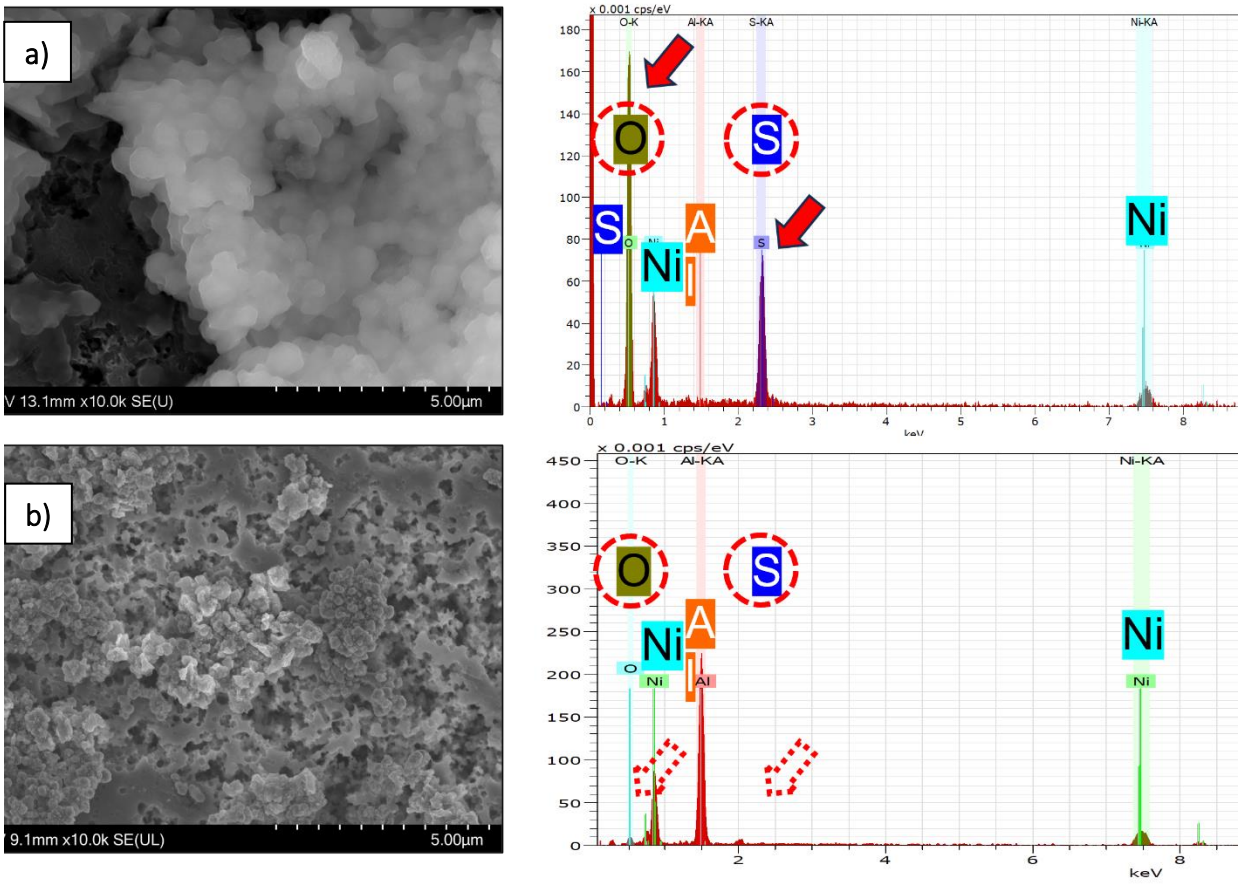

Figure 4-3 EDS analysis of solution coated sample a) before reduction and b) after reduction

4.3.2 Distribution of Nickel nanoparticles

The final yield of the CNTs on the substrate (mg/cm^2) is directly proportional to the mass of Ni available on the substrate, in the form of active and discrete nanoparticles. Hence, the morphology and distribution were studied by SEM, and the mass loading of Ni on each substrate was determined by simple and sensitive weighing.

The topological SEM analysis (Figure 4-4) shows that the Ni nanoparticles/clusters are packed densely and uniformly over the entire surface of the sputtered Al foil (Figure 4-4a). However, the drop coated and 4×dip coated samples (Figure 4-4c,d) show non-uniform and distribution and incomplete coverage on the etched aluminium foil. The spray coated and 1×time dip coated samples (Figure 4-4b,e) show a further inadequate surface coverage. These images suggest that the mass loading of the Ni varies significantly among different samples, which will be quantified in the next sub-section.

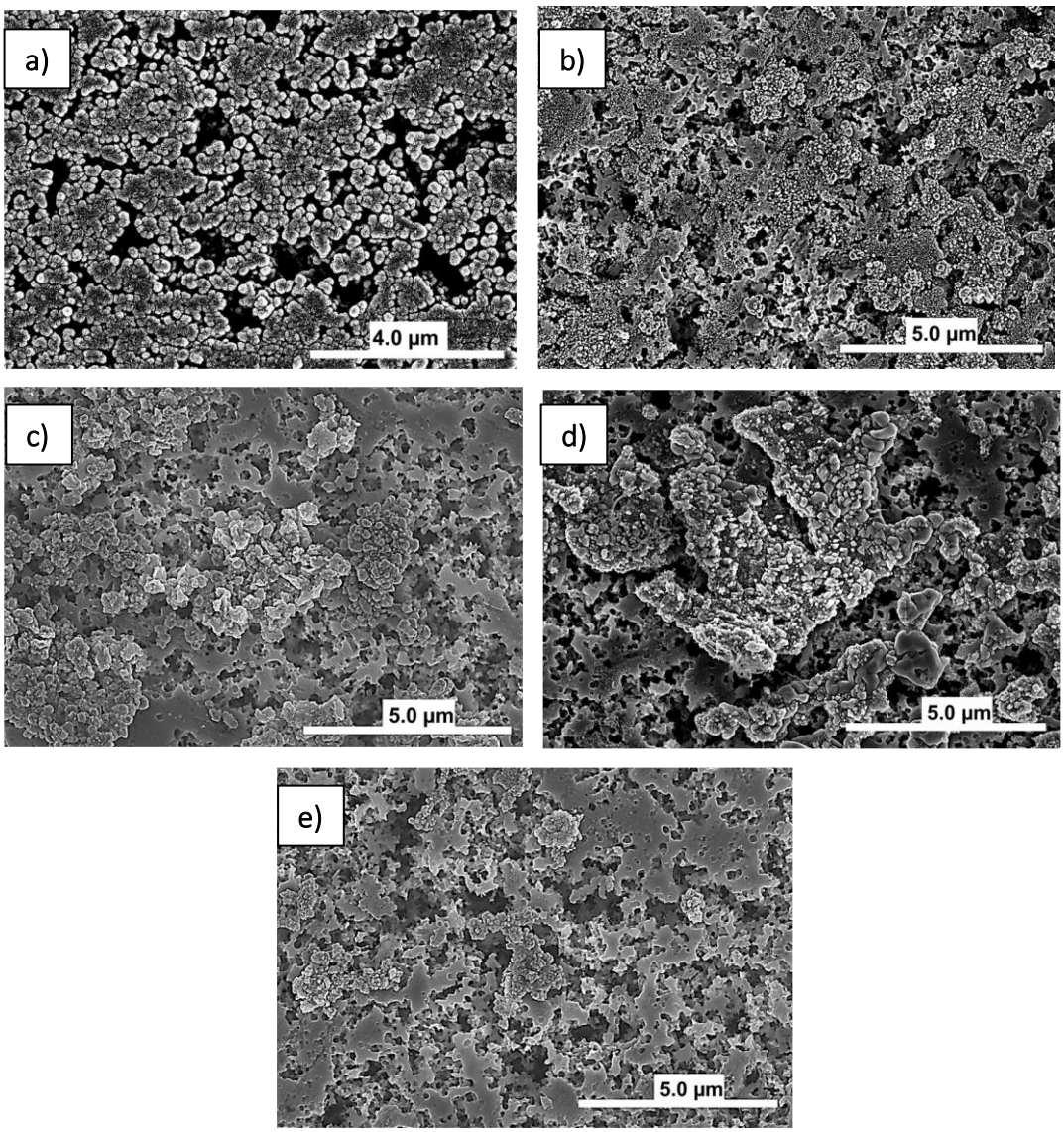

Figure 4-4 SEM images of a) sputtered, b) Spray coated, c) Drop coated, d) 4 times Dip coated and e) 1 time Dip coated samples.

However, considering the adhesion of CNT, EDS mapping were performed in order to analyse the distribution of nanoparticles along the porous area of the aluminium substrate.

Figure 4-5 shows the EDX mapping of Ni nanoparticles on the sputtered sample (Figure 4-5a) and a solution-coated sample (Figure 4-5b). For the sputtered sample, a thin layer of nickel is distributed uniformly on the surface of the substrate with very little sub-surface penetration into the etch pits. On the other hand, Ni particles are sparsely distributed on the surface of the solution-coated sample but have penetrated into the deepest pores/etch pits on the aluminum foil.

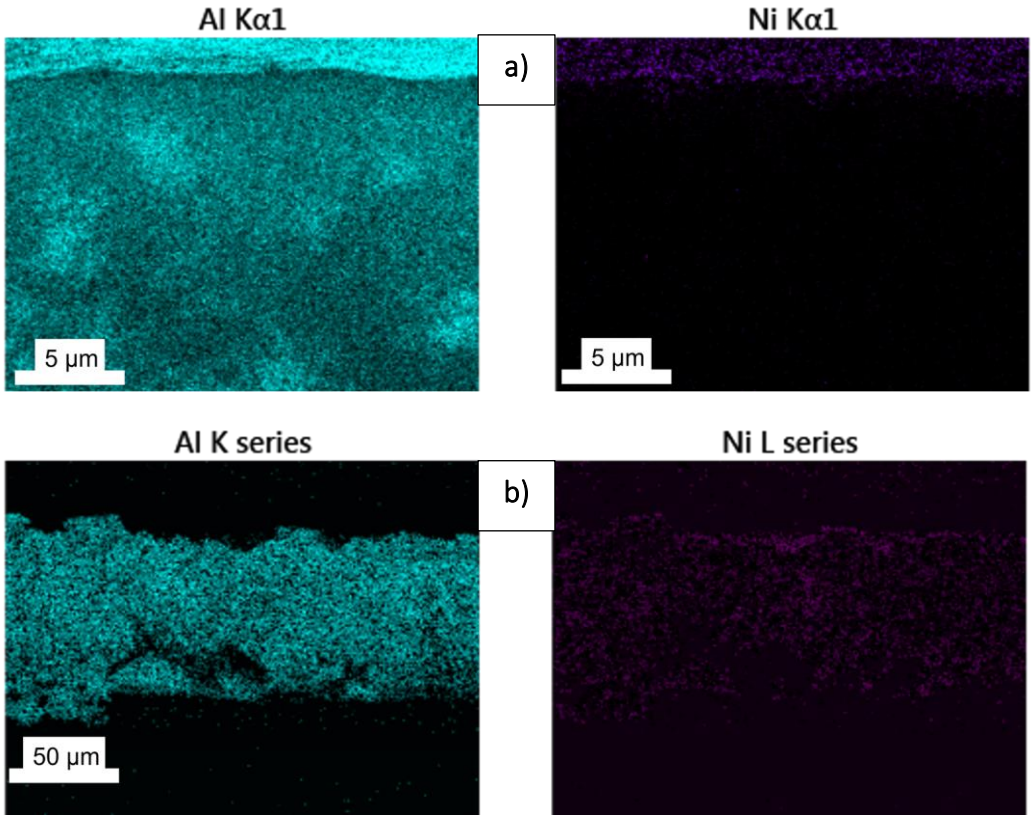

Figure 4-5 Mapping of Nickel distribution a) Sputtered sample and b) Solution coated sample.

The depth of penetration of Ni nanoparticles is vital for good adhesion of the CNT film that grows during the CVD on the Al foil. Ni nanoparticles present in the subsurface pits of the solution-coated sample mediate strong anchoring between the foil and the CNTs. Figure 4-6 shows that upon performing CVD under the same conditions, the CNTs grown on the solution-coated sample (Figure 4-6a) exhibit excellent adhesion, whereas that on

the sputtered samples (Figure 4-6b,c) show delamination of the CNT films, which is especially predominant when the mass loading of CNTs increases.

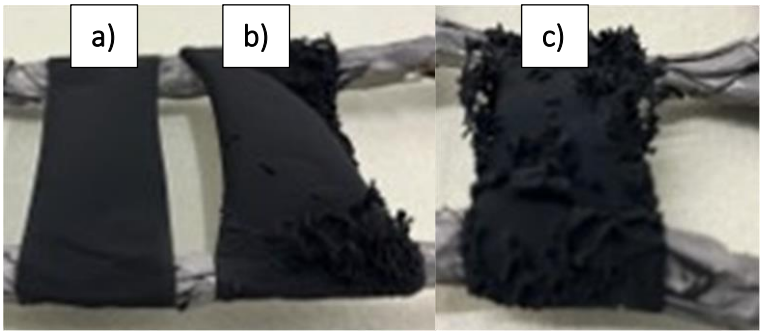

Figure 4-6 Samples after CVD a) solution coated, b & c) Sputtered.

4.3.3 Nickel mass loading differentiation

The mass loading of nickel particles was measured by subtracting the mass of the aluminium foil before and after the deposition process. This study mainly focused on the 300 nm thick nickel layer sputtered samples and all solution coated samples, as these samples showed the best growth kinetics among others (10-250 nm sputtered Ni layers that were investigated simultaneously). The data (Figure 4-7) was prepared though averaging the masses of random number of samples from each category. For the uniform distribution through sputtering process the mass loading was much higher than solution coated sample which also led to synthesis of densely packed CNTs with higher gravimetric capacitance.

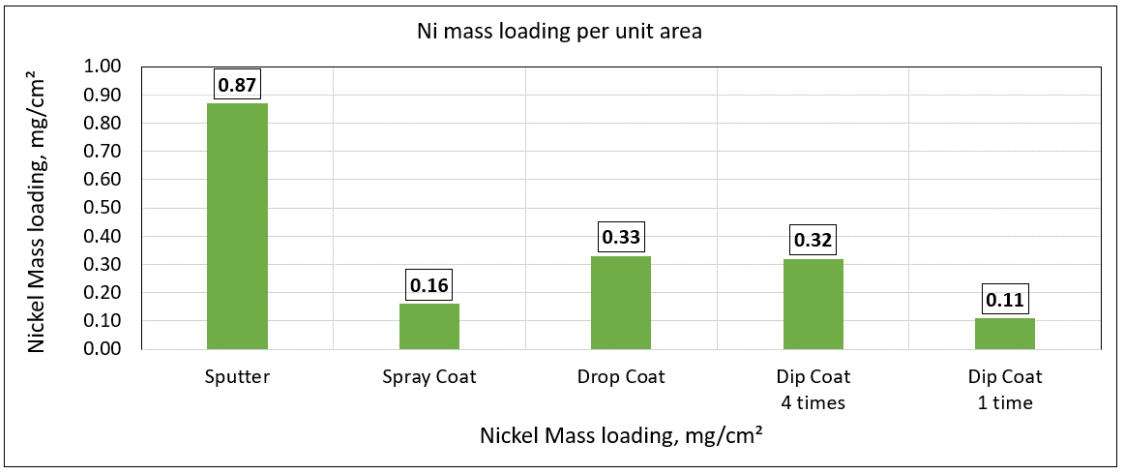

Figure 4-7 Mass loading of Nickel nanoparticles from different deposition methods

4.3.4 Effects of deposition method on Mass Loading of carbon nanotube (CNT)

Mass loading of carbon nanotubes were carried out and the measured data (Figure 4-8) were compared for samples prepared in different methods. This study verified the dependence of CNT growth on the amount of nickel nanoparticles present in the sample.

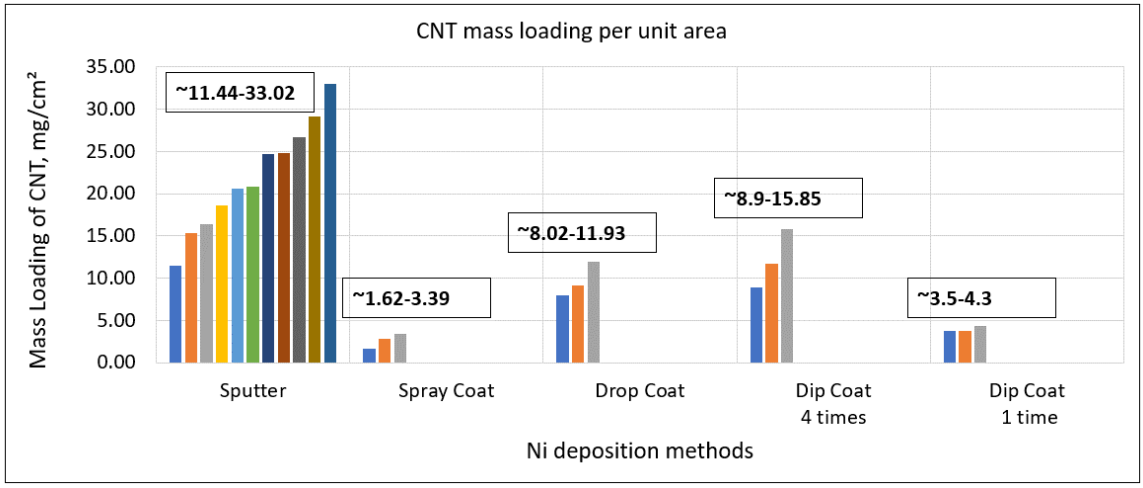

Figure 4-8 Mass loading of CNTs respect of deposition methods

As expected, the CNT mass loading is highest for sputtered samples which varied from 11-33 mg/cm², were the highest amount of nickel is present. For the 4 times dip coated and drop coated sample the values are ranging from 8-16 mg/cm² which also had an intermediate amount of nickel loading. The least nickel loaded samples, 1 time dip coated, and spray coated samples exhibited CNT mass loading around 1.5-4.3 mg/cm².

4.3.5 Effects of deposition method on the Capacitance

Electrochemical analysis was performed on different samples with 2-electrode method where the current and voltage were measured, and the areal capacitance was calculated.

$$C = \frac{\int_0^V idv \times 2 \times 1000}{2V_s \Delta V A_E} \quad (3)$$

Here,

C= Areal capacitance, mF/cm²

V= Applied voltage

i= Instantaneous current

Vs= Scan rate, 5 mv/s

ΔV= Standard potential for organic electrolyte, 2.7 V [30]

The areal capacitance of the electrodes, thus measured, are presented and compared in Figure 4-9.

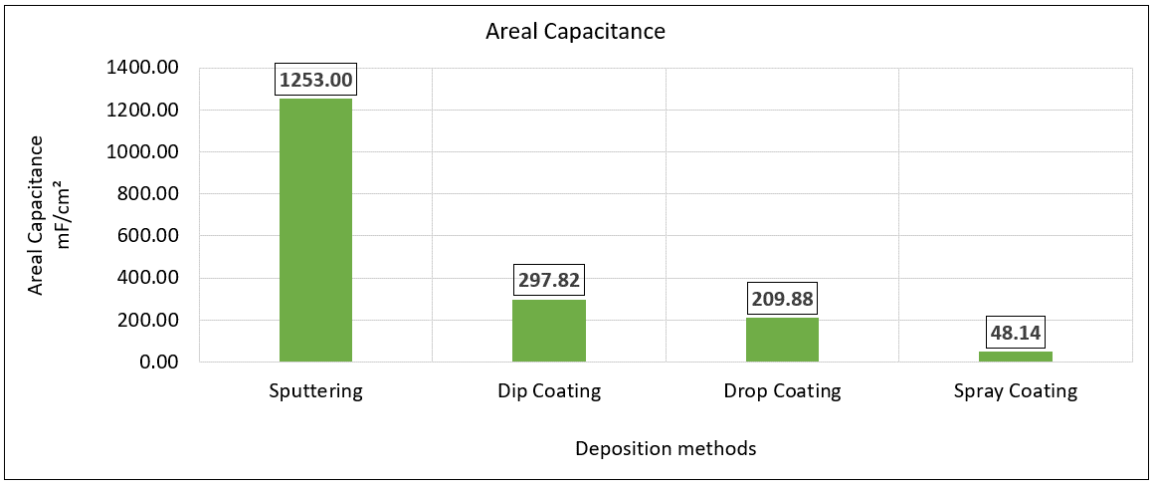

Figure 4-9 Areal capacitance of electrodes produced on samples prepared by different Nickel deposition methods.

A phenomenally high areal capacitance of 1253 mF/cm^2 for sputtered samples is attributed to the presence of densely distributed nanoparticles compared to the solution coated samples. Interestingly, the mass loading of CNTs on the sputtered samples is merely 16 mg/cm^2. At mass loadings above 20 mg/cm^2, CNTs usually get delaminated (Figure 4-6).

4.4 Optimized Growth of CNTs On Nickel Coated Al Foil

The ratios of gas mixture (Ar, H_2, C_2H_2) were systematically varied in order to analyse the influence of their concentrations and flowrates on the CNT growth process. By carefully adjusting the ratios and flowrates of each precursor gas to investigate the effects of different gas compositions on the characteristics and properties of the synthesized CNTs. For the catalyst deposition, dip-coating method was chosen and evaluated where samples underwent 4 times dip-coating cycles. This method was selected for its advantages of being quick, easy, cost-effective, and scalable. Furthermore, the adhesion and uniformity of the CNTs grown on these samples were found to be excellent.

This approach enabled a detailed examination of the relationship between precursor gas parameters and the resulting CNT growth, providing valuable insights for optimizing the CNT synthesis process.

4.4.1 Effect of H_2 proportion on the CNT growth characteristics

In the context of carbon nanotube (CNT) growth, hydrogen gas plays a crucial role in activating catalytic nickel particles, which act as nucleation sites for CNT formation. Additionally, hydrogen gas can be utilized during the etching and purification processes in CNT growth. It reacts with amorphous carbon and carbonaceous impurities, facilitating their removal from the catalyst surface and enhancing the overall purity of the CNTs produced.

The concentration of hydrogen can be adjusted to stimulate CNT growth, and its effect was specifically tested in this study by varying its proportion while keeping the other precursors unchanged. The influence of hydrogen on CNT growth was evaluated by altering its concentration, and the approach is documented in *Table 4-1*. This experimental approach allowed for a systematic investigation of the impact of hydrogen on CNT growth, enabling to optimize the conditions for achieving desired CNT properties.

Table 4-1 Varied Hydrogen proportion for CNT growth

C_2H_2 (SCCM)	H_2 (SCCM)	Ar (SCCM)	Gas Ratio
90	**0**	**180**	**1:0:2**
90	**350**	**180**	**1:3.8:2**
90	**450**	**180**	**1:5:2**

In the initial condition, when hydrogen was absent during the synthesis process, the growth of carbon nanotubes (CNTs) was barely observable (Figure 4-10a). However, there were carbon depositions present on the substrate, but it was challenging to distinguish them as actual CNTs. This occurrence may have been a result of excessive oxidation of the nickel particles used as catalysts.

Subsequent experiments were conducted by increasing the flow of hydrogen to 350 SCCM and 450 SCCM (Figure 4-10b,c). Under these conditions, it became possible to identify the presence of CNTs. The introduction of higher hydrogen flow rates facilitated the growth and formation of distinct CNT structures. This observation indicates the crucial role of hydrogen in promoting the proper growth and development of CNTs during the synthesis process.

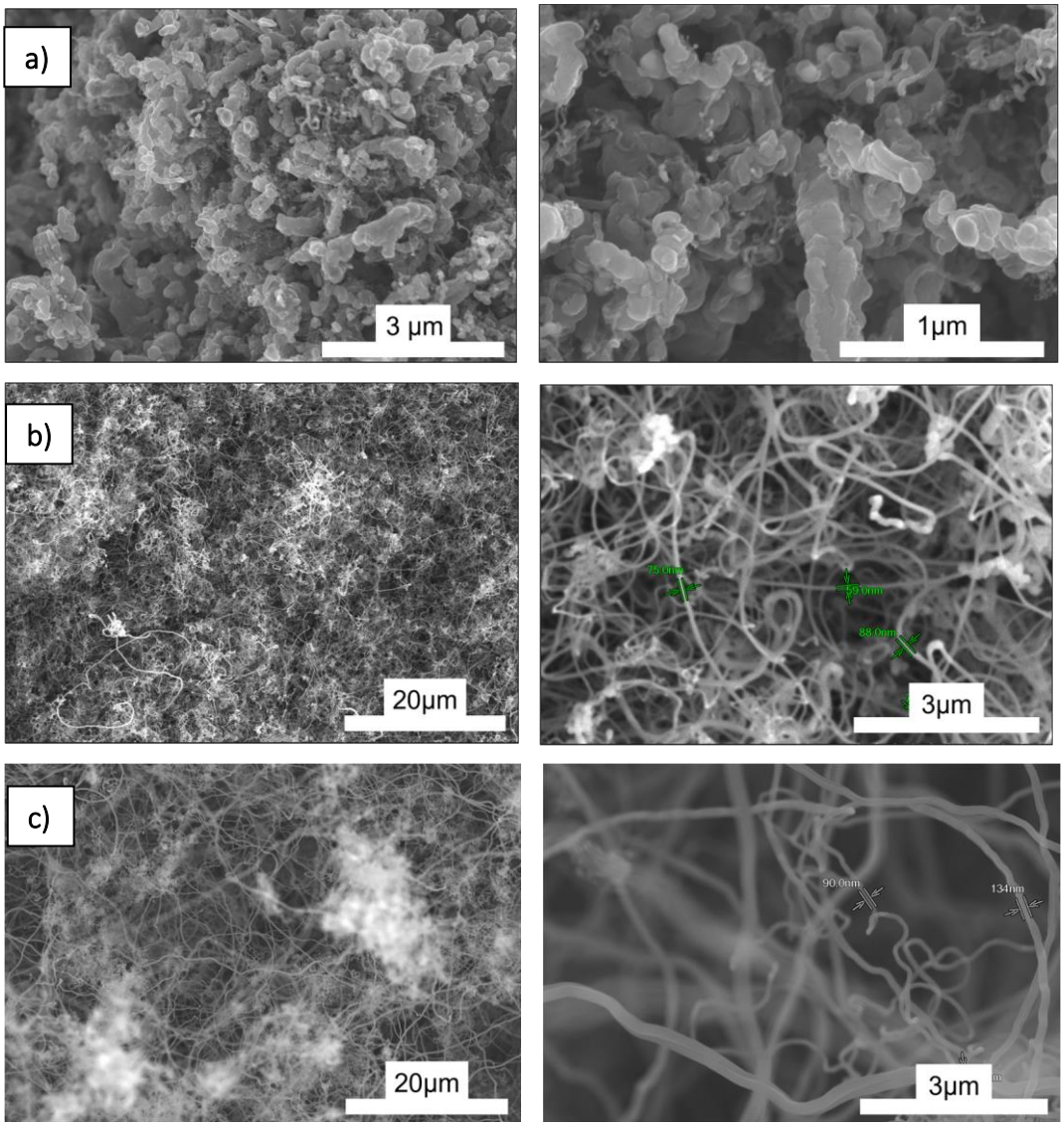

Figure 4-10 SEM images of after synthesis samples with a) 0 SCCM Hydrogen, b) 350 SCCM Hydrogen and c) 450 SCCM Hydrogen

During the electrochemical testing by 2-electrode method at 5mV/s scan rate, of the synthesized CNT based coin cells, it was observed that the capacitance increased as the proportion of H_2 increased. This finding suggests that the properties of CNTs synthesized with a higher amount of H_2 improved, indicating enhanced electrochemical performance.

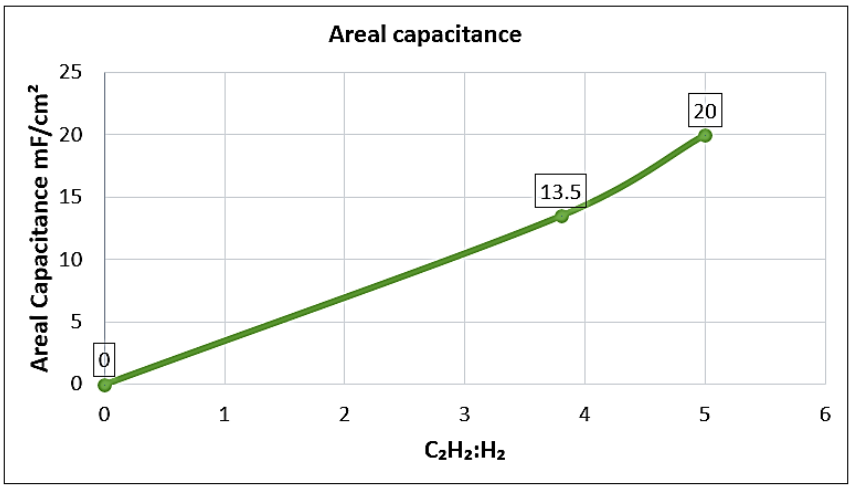

Figure 4-11 Areal capacitance of electrodes with different proportion of Hydrogen

However, when comparing the areal capacitance values of electrodes prepared with 350 SCCM and 450 SCCM of H_2, the difference was not significant (Figure 4-11). This observation led to select both proportions of H_2 for further investigation when studying the effects of all three precursors.

4.4.2 Effect of gas flow rate on the CNT growth characteristics

In this section of the study, the effects of gas flow rate on carbon nanotube (CNT) synthesis were investigated. The evaluation of the synthesized CNT electrodes involved assessing the mass loading and areal capacitance to examine the differences and quality of the electrodes. To conduct the capacitance tests, a 3-electrode method was employed with a scan rate of 100 mV/s. The experiments involved varying gas ratios, concentrations, and flow rates, which are detailed in *Table 4-2*. These parameters were systematically adjusted to analyse their impact on CNT synthesis and optimize the growth process.

Table 4-2 Concentration and flowrate variation for CNT synthesis

C_2H_2 (SCCM)	H_2 (SCCM)	Ar (SCCM)	Gas Ratio (C_2H_2:H_2: Ar)	Flowrate/ area (ml/min/cm²)	Flowrate (C_2H_2) / area (ml/min/cm²)
90	450	180	1:5:2	1.26	0.16
200	1000	400	1:5:2	2.79	0.35
229	1000	458	1:4.4:2	2.95	0.40
266	1000	532	1:3.8:2	3.14	0.46
366	1000	732	1:2.7:2	3.66	0.64
166	624	332	1:3.8:2	1.99	0.29

The mass loading analysis confirmed the obvious relationship between the flow rate of C_2H_2 and the yield of carbon nanotubes. As the flow rate of C_2H_2 increased, the CNT yield also increased naturally due to the higher concentration of the precursor gas. This trend is illustrated in Figure 4-12, where the highest CNT yield was achieved at the highest flow rate of C_2H_2.

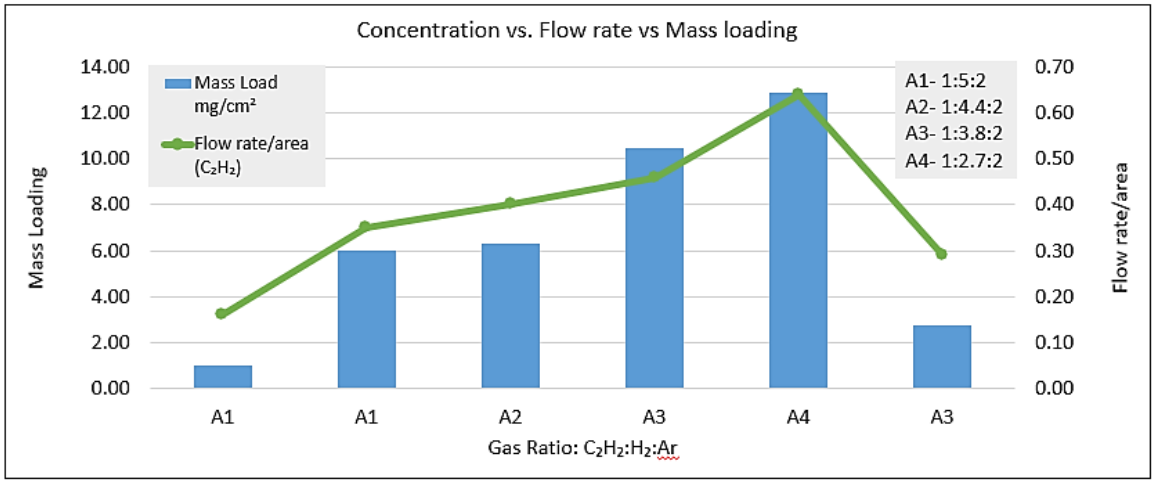

Figure 4-12 Mass loading of CNT at different flowrates and gas ratios

Subsequent electrochemical tests conducted on the synthesized carbon nanotube (CNT) electrodes unveiled an interesting finding. Although the areal capacitance of the

electrodes was found to increase with the increasing flow rate of the precursors (Figure 4-13), it then started to decline with a further increase. Additionally, the adherence of the CNTs to the substrate decreased as well. This observation indicated that the flow rate of acetylene needs to be set at an optimum value for achieving the highest capacitance.

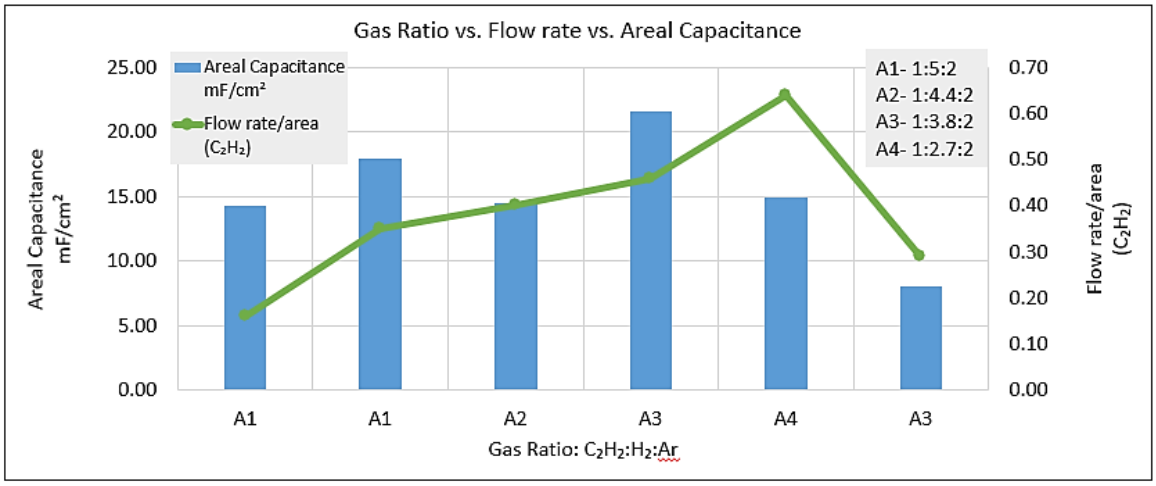

Figure 4-13 Areal Capacitance of CNT at different flowrates and gas ratios

As previously mentioned, the proportion of hydrogen in the gas mixture plays a crucial role in the synthesis of carbon nanotubes and can affect the formation of amorphous or disordered carbon. In order to investigate the reason for the lower capacitance observed when the flowrate was increased beyond the ratio of 266:1000:532 (C_2H_2:H_2:Ar), Fourier-transform infrared spectroscopy (FTIR) was performed on both samples. The FTIR spectra (Figure 4-14) provided valuable insights into the molecular structure of the samples. The band within the range of 1300-1515 $\mathbf{cm^{-1}}$ corresponds to C-H bonds from a mixture of sp^2-sp^3 hybridization (mixed carbon), while the band within the range of 500-1000 $\mathbf{cm^{-1}}$ corresponds to C=C bonds from sp^2 hybridization, which is the backbone of CNTs [31]. Upon analysis of the FTIR spectra, it was observed that the curve representing the lower flowrate of 266 SCCM exhibited a lower transmittance for the SP^2 bands (790 cm^{-1} and 2109 cm^{-1}) compared to the curve from the higher flowrate of 366 SCCM (802 cm^{-1} and 2120 cm^{-1}). This indicates that the amount of SP^2 bonds (C=C) in the sample grown with 266 SCCM acetylene is higher compared to the one grown with 366 SCCM acetylene. Furthermore, the transmittance of the sample grown with 366 SCCM acetylene is lower in the range where mixed carbon is shown (1300-1515 cm^{-1}). This suggests that although

the mass of carbon is higher with a flowrate of 366 SCCM, a large proportion of this carbon is in disordered state, rather than exhibiting sp^2 hybridization.

Based on these findings, it can be speculated that the higher amount of amorphous carbon in the sample with increased flowrate and decreased H_2 concentration leads to a decrease in capacitance, despite an increase in mass loading. The presence of disordered carbon can adversely affect the electrochemical performance of the electrodes and result in lower capacitance values.

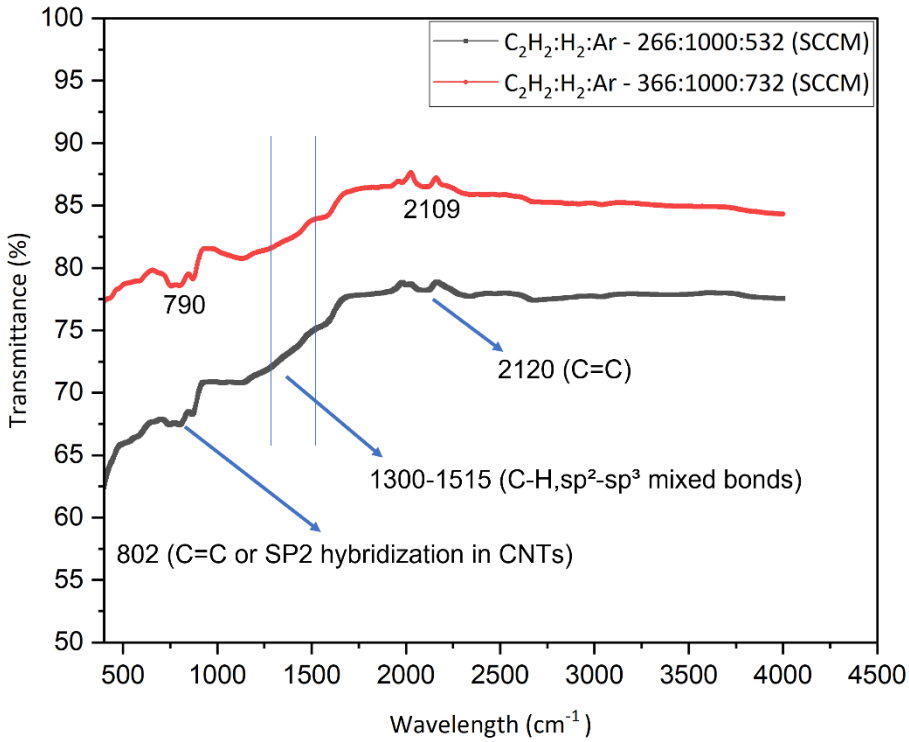

Figure 4-14 FTIR spectra for CNTs and amorphous carbon at different flowrates

These observations led to the conclusion that the gas ratio and concentration of all three precursors significantly impact the electrochemical properties of the electrodes.

These results highlight the intricate relationship between precursor flow rates and the resulting electrochemical performance of the electrodes. In addition, optimizing the gas ratio and concentration of the precursors is crucial for achieving desirable electrochemical properties, such as high capacitance and strong adhesion of the CNTs to the electrodes.

4.4.3 Effect of growth duration on the CNT yield and capacitance

The influence of growth duration on CNT synthesis was investigated by varying the synthesis time from 15 to 60 minutes. The analysis revealed interesting trends in both the mass loading and areal capacitance of the synthesized CNTs. The areal capacitance was measured through 2-electrode testing method at 5mV/s.

As the synthesis time increased, the mass loading of CNTs also increased. This suggests that a longer synthesis duration allows for more CNTs to be grown and deposited on the substrate. However, the areal capacitance of the CNT electrodes showed a different behaviour which were conducted through 3-electrode test at 100mV/s. After reaching a peak at 30 minutes of synthesis, the areal capacitance saturated and did not significantly increase with further synthesis time. This saturation indicates that the electrochemical performance of the electrodes reaches a maximum at this specific synthesis duration. The growth rate of CNTs during synthesis is highest at the beginning and gradually decreased with increasing synthesis time [32]. This indicates that the initial stages of CNT growth are more rapid compared to later stages.

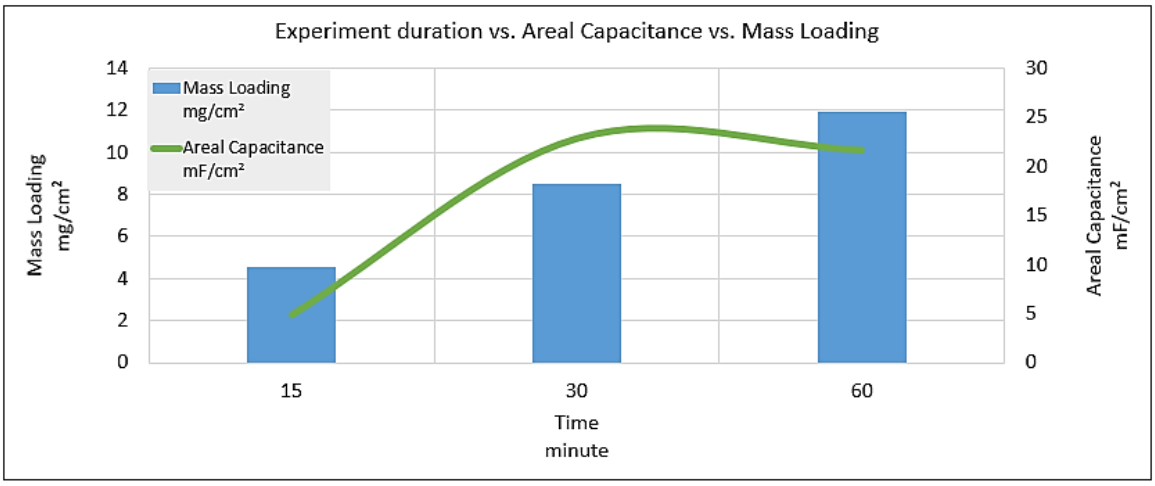

Figure 4-15 Mass loading and Areal capacitance of CNT electrodes with varying synthesis time.

These findings emphasize the importance of optimizing the synthesis time to achieve the desired balance between mass loading, areal capacitance, and growth rate of CNTs. The optimized growth duration for the selected recipe has hence been fixed to 30 minutes.

4.4.4 Growth of CNTs with optimized conditions for application in EDLCs

By consolidating the findings from the aforementioned experiments, further investigations were conducted using the optimized synthesis conditions. These conditions were expected to yield the highest carbon nanotube (CNT) production while maintaining good adhesion and superior electrochemical properties. One notable observation was the outstanding areal capacitance exhibited by the sputtered samples in comparison to the other samples that underwent different catalyst deposition methods. This highlights the importance of the synthesis process conditions in determining the properties of the synthesized CNTs (Table 4-3).

Table 4-3 Optimal Condition for CNT synthesis and CNT properties

Parameters	Values
C_2H_2:H_2:Ar (SCCM)	**266:1000:532**
Temperature (℃)	**580**
Pressure (atm)	**1**
Synthesis Time (min)	**30**
Mass loading (mg/cm²)	**16**
Carpet Height (µm)	**120**
Areal Capacitance (mF/cm²)	**1253**
Gravimetric Capacitance (F/g)	**78**

The evaluation of the process conditions and properties of the synthesized CNTs provides valuable insights into their quality and suitability for various applications. By carefully optimizing the synthesis conditions, it was possible to achieve the desired CNT yield, adhesiveness, and electrochemical properties necessary for the intended applications.

SEM analysis was conducted to investigate the morphological aspects of CNT growth, focusing on diameter distribution, uniformity, and adhesion. The results revealed that the diameter of the CNTs varied within the range of 30-150 nm (Figure 4-16), which was consistent across all samples with similar diameter distributions.

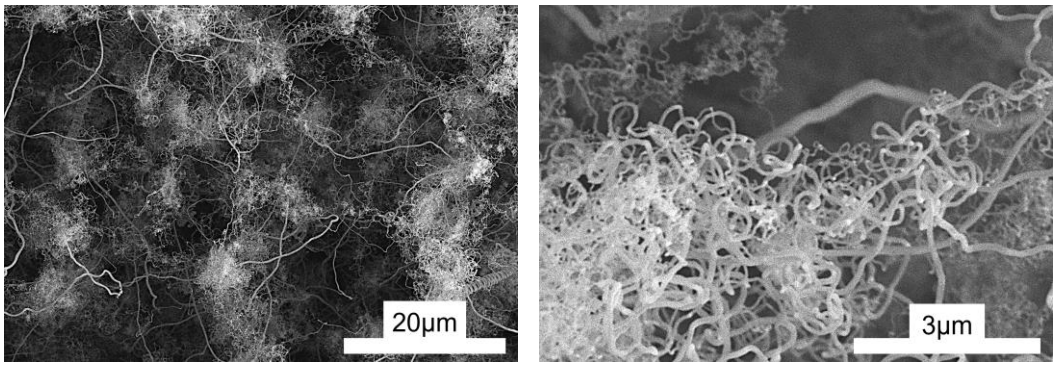

Figure 4-16 SEM images of CNTs on sputtered sample at different magnifications

However, as mentioned previously, the CNTs grown on the sputtered samples exhibited distinct characteristics of delamination with increasing growth. This phenomenon limited the overall uniformity of the samples, as the growth of CNTs became less consistent compared to the solution-coated samples. Despite of these facts, this sample demonstrated good adhesion under the optimal parameters.

The packing density of the CNTs grown on sputtered samples was calculated by dividing the mass loading with the volume of CNTs (per sq. cm) and compared with that of the best samples produced on the lab scale CVD reactor (Table 4-4).

Table 4-4 Comparison of Packaging Density

	Mass loading of CNTs (mg/cm^2)	Average carpet height (µm)	Volume of CNTs per sq. cm (cm^3)	Packing density of CNTs (g/cc)	Areal Capacitance (mF/cm^2)	Gravimetric capacitance (F/g)
Sputtered Sample (Pilot Scale)	**16.00**	**120.00**	**0.012**	**1.3**	**1253**	**78**
Drop-coated Sample (Lab Scale)	**53.14**	**1450.00**	**0.145**	**0.37**	**2471**	**53**

Now, comparing both samples, it can be observed that the packing density of CNTs produced with a sputtered sample on the large CVD reactor is approximately 3.5 times higher than that produced with a drop-coated sample on the small CVD reactor.

This higher packing efficiency in the large CVD reactor resulted in an outstanding capacitance, as follows:

The areal capacitance = 1253 mF cm^{-2} at 5 mV s^{-1} (Figure 4-17)

The gravimetric capacitance = 1253 mF/16 mg = 78 F g^{-1}

The higher packing density of CNTs in the sputtered samples is attributed to the higher packing density of Ni nanoparticles.

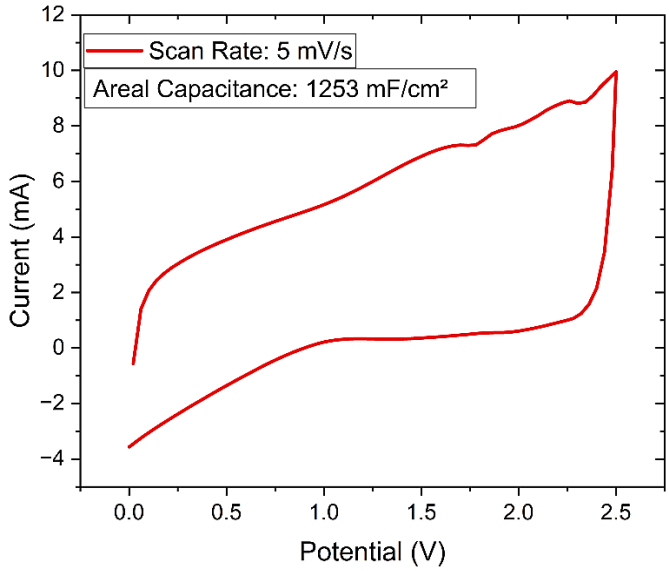

Figure 4-17 Areal Capacitance at 5mV/s scan rate

Furthermore, in order to assess the electrochemical performance of the synthesized CNT electrodes, a comparison was made with state-of-the-art activated carbon (AC) based electrodes. The results of the comparison demonstrated a phenomenal outcome for this study. Both the areal capacitance and gravimetric capacitance of the CNT electrodes synthesized at pilot/industrial level surpassed the best values available in recent times for AC-based electrodes (Figure 4-18). This suggests that the synthesized CNT electrodes have superior electrochemical properties and exhibit higher areal and gravimetric capacitances.

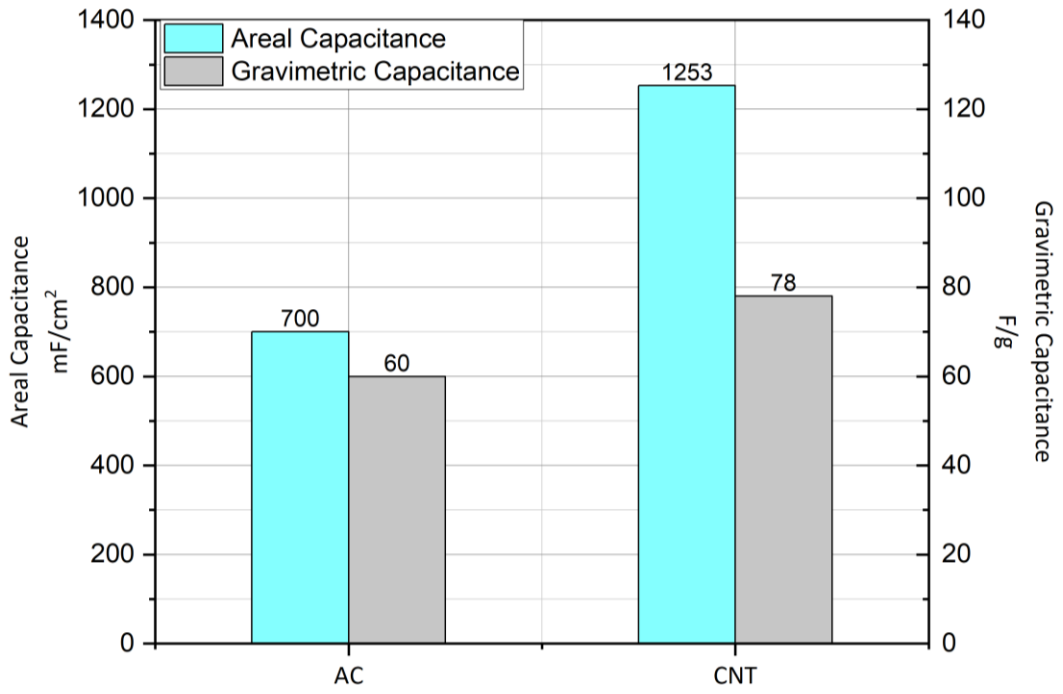

Figure 4-18 Comparison between activated carbon and CNT based electrodes regarding Capacitance.

It is to be noted that the best state-of-the-art AC electrodes exhibit only 60 F/g and 700 mF/cm^2, whereas our method resulted in an outstanding value of 78 F/g and 1253 mF/cm^2. These findings highlight the potential of the iCL-CNT electrodes as a viable alternative to traditional activated carbon electrodes in both stationary and mobile applications.

5 Conclusions and Future Work

In conclusion, this study focused on the development of a synthesis process for carbon nanotubes (CNTs) using a pilot-scale or industrial-scale facility. The initial phase involved understanding and optimizing the functionality of the reactor, which presented challenges due to differences compared to the lab scale reactor. The study successfully designed and developed a process that ensured the required temperature inside the reactor, a critical factor for atmospheric chemical vapor deposition (APCVD).

The reduction process for the solution-coated samples was successfully carried out, reducing the nickel salt to nickel nanoparticles, essential for CNT growth. Mass loading and nickel distribution studies revealed that the nanoparticles were uniformly and densely distributed in the sputtered samples, while they were sparsely distributed on the porous surface of the aluminum substrate in the solution-coated samples. Solution-coated samples exhibited excellent adhesion, but poor packing density of CNTs, whereas the sputtered samples resulted in excellent packing density of CNTs but a poor adhesion.

The study then focused on optimizing the CNT synthesis process by evaluating the effects of different proportions of hydrogen gas. The presence of H_2 was found to be crucial for CNT growth and the attainment of superior physical and electrochemical properties. The optimum ratio was found to be 3.8 times the flowrate of acetylene.

The effects of gas ratio, concentration, flowrate, and synthesis time were investigated. It was observed that the optimal gas ratio was (1:3.8:2) C_2H_2:H_2:Ar, and a flowrate of 266:1000:532 SCCM was determined to be the best. The synthesis time was optimized to 30 minutes, as the electrochemical performance did not improve further and delamination of CNTs occurred with increased growth time.

CNT electrodes synthesized under above optimized conditions exhibited a phenomenally high areal capacitance of 1253 mF/cm² combined with an outstanding gravimetric capacitance of 78 F/g, surpassing the performance of best state-of-the-art activated carbon (AC) based electrodes with areal capacitance of 700 mF/cm² and gravimetric capacitance of 60 F/g. While the areal capacitance of the CNT electrodes was smaller than those synthesized in the lab scale reactor, the higher gravimetric capacitance and 3.5 times higher packaging density were achieved.

These results suggest that this study successfully optimized the synthesis process for iCL-CNTs in a pilot-scale or industrial-scale facility and the electrodes developed on this pilot

scale reactor are suitable for both stationary (electronics, smart cards) and mobile (automobiles, marine) applications, as well as for making flexible cells with size constraints.

Future work

In addition to the findings discussed in this paper, it is worth mentioning that the study considered the potential of water-assisted chemical vapor deposition (WA-CVD) for CNT synthesis. However, due to time constraints, the data evaluation regarding WA-CVD was inconclusive and not included in this paper. Future research could focus on a detailed investigation of the effects of WA-CVD on CNT synthesis.

Furthermore, exploring scalable and more conformal methods for catalyst deposition is an important aspect to be studied. Techniques such as etching of CNTs and nitrogen (N_2) doping can be evaluated, as they are speculated to be effective in increasing the surface area of the CNTs. This increased surface area can potentially lead to superior electrochemical performance of the CNT-based electrodes.

Additionally, further optimization and study of the pilot-scale reactor are recommended. This optimization process could contribute to the production of high-quality CNT-based electrodes in a shorter time, at a lower cost, and with improved environmental sustainability.

In summary, this study provides a solid foundation for future research directions. These efforts could lead to the development of efficient and scalable manufacturing processes for CNT-based electrodes, facilitating their broader application in various fields.

References/bibliography

[1] Raza, W., Ali, F., Raza, N., Luo, Y., Kim, K.-H., Yang, J., Kumar, S., Mehmood, A., & Kwon, E. E. (2018). Recent advancements in supercapacitor technology. Nano Energy, 52, 441–473.

[2] Gidwani, M., Bhagwani, A., & Rohra, N. (2014). Supercapacitors: the near Future of Batteries.

[3] Zhang, C.-J. (2018). Super pseudocapacitors. 3(12), 1019–1019.

[4] Chen, T., & Dai, L. (2013). Carbon nanomaterials for high-performance supercapacitors. Materials Today, 16(7-8), 272–280.

[5] Kroto, H. W., Heath, J. R., O'Brien, S. C., Curl, R. F., & Smalley, R. E. (1985). C60: Buckminsterfullerene. Nature, 318(6042), 162–163.

[6] Iijima, S. (1991). Helical microtubules of graphitic carbon. Nature, 354(6348), 56–58.

[7] Saifuddin, N., Raziah, A. Z., & Junizah, A. R. (2013). Carbon Nanotubes: A Review on Structure and Their Interaction with Proteins. Journal of Chemistry, 2013, 1–18.

[8] Iijima, S., & Ichihashi, T. (1993). Single-shell carbon nanotubes of 1-nm diameter. Nature, 363(6430), 603–605.

[9] Bethune, D. S., Kiang, C. H., de Vries, M. S., Gorman, G., Savoy, R., Vazquez, J., & Beyers, R. (1993). Cobalt-catalysed growth of carbon nanotubes with single-atomic-layer walls. Nature, 363(6430), 605–607.

[10] Maheswaran, R., & Shanmugavel, B. P. (2022). A Critical Review of the Role of Carbon Nanotubes in the Progress of Next-Generation Electronic Applications. Journal of Electronic Materials, 51(6), 2786–2800.

[11] Prasher, R. S., Hu, X. J., Chalopin, Y., Mingo, N., Lofgreen, K., Volz, S., Cleri, F., & Keblinski, P. (2009). Turning Carbon Nanotubes from Exceptional Heat Conductors into Insulators. Physical Review Letters, 102(10).

[12] Carlson, D. E., & Wronski, C. R. (1976). Amorphous silicon solar cell. Applied Physics Letters, 28(11), 671–673.

[13] H.M. Manasevit. (1981). Recollections and reflections of MO-CVD. 55(1), 1–9.

[14] Choy, K. (2003). Chemical vapour deposition of coatings. Progress in Materials Science, 48(2), 57–170.

[15] Yan, K., Fu, L., Peng, H., & Liu, Z. (2013). Designed CVD Growth of Graphene via Process Engineering. Accounts of Chemical Research, 46(10), 2263–2274.

[16] Hatta, M. N. M., Hashim, M. S., Hussin, R., Aida, S., Kamdi, Z., Ainuddin, A., & Yunos, M. (2017). Synthesis of carbon nanostructures from high density polyethylene (HDPE) and polyethylene terephthalate (PET) waste by chemical vapour deposition. Journal of Physics: Conference Series, 914, 012029.

[17] Fraga, M., & Pessoa, R. (2020). Progresses in Synthesis and Application of SiC Films: From CVD to ALD and from MEMS to NEMS. Micromachines, 11(9), 799.

[18] Drosos, C., & Vernardou, D. (2015). Perspectives of energy materials grown by APCVD. Solar Energy Materials and Solar Cells, 140, 1–8.

[19] Endo, M., Hayashi, T., Kim, Y. A., & Muramatsu, H. (2006). Development and Application of Carbon Nanotubes. Japanese Journal of Applied Physics, 45(6A), 4883–4892.

[20] Wang, X.-D., Vinodgopal, K., & Dai, G.-P. (2019). Synthesis of Carbon Nanotubes by Catalytic Chemical Vapor Deposition. Perspective of Carbon Nanotubes.

[21] Kumar, M. (2011). Carbon Nanotube Synthesis and Growth Mechanism. Carbon Nanotubes - Synthesis, Characterization, Applications. https://doi.org/10.5772/19331

[22] Shah, K. A., & Tali, B. A. (2016). Synthesis of carbon nanotubes by catalytic chemical vapour deposition: A review on carbon sources, catalysts and substrates. Materials Science in Semiconductor Processing, 41, 67–82.

[23] Kumar, M., Keita Kakamu, Okazaki, T., & Ando, Y. (2004). Field emission from camphor–pyrolyzed carbon nanotubes. 385(3-4), 161–165.

[24] Kumar, M., & Ando, Y. (2003). A simple method of producing aligned carbon nanotubes from an unconventional precursor – Camphor. Chemical Physics Letters, 374(5-6), 521–526.

[25] Li, D., & Tong, L. (2020). Direct Growth of Carbon Nanotubes on Aluminum Foil by Atmospheric Pressure Microwave Plasma Chemical Vapor Deposition. Processes, 9(1), 36.

[26] Kim, S. U., Pint, C. L., Amama, P. B., Zakharov, D. N., Hauge, R. H., Maruyama, B., & Stach, E. A. (2010). Evolution in Catalyst Morphology Leads to Carbon Nanotube Growth Termination. 1(6), 918–922.

[27] Huang, Z. P., Wang, D. Z., Wen, J. G., Sennett, M., Gibson, H., & Ren, Z. F. (2002). Effect of nickel, iron and cobalt on growth of aligned carbon nanotubes. Applied Physics A: Materials Science & Processing, 74(3), 387–391.

[28] Chaudhari, M. N. (2021). Thin film Deposition Methods: A Critical Review. International Journal for Research in Applied Science and Engineering Technology, 9(VI), 5215–5232.

[29] DU, Kang, CHEN, Xuyuan, and ØHLCKERS, Per Alfred, "Direct growth cross linked carbon nanotubes on microstructured metal substrate for supercapacitor application," WO 2022/078759 A1, Apr. 21, 2022

[30] Volfkovich, Yu. M. (2021). Electrochemical Supercapacitors (a Review). Russian Journal of Electrochemistry, 57(4), 311–347.

[31] Ţucureanu, V., Matei, A., & Avram, A. M. (2016). FTIR Spectroscopy for Carbon Family Study. Critical Reviews in Analytical Chemistry, 46(6), 502–520.

[32] Patole, S. P., Alegaonkar, P. S., Lee, H.-C., & Yoo, J.-B. (2008). Optimization of water assisted chemical vapor deposition parameters for super growth of carbon nanotubes. Carbon, 46(14), 1987–1993.

List of Tables and Figures